Global Biogeochemical Cycles

RESEARCH ARTICLE
10.1029/2025GB009031

Iron and Manganese Cycling in the Atlantifying Barents Sea: Concentrated Inputs and Emerging Limitations

R. Hawley[1], C. Mahaffey[2], J. Hopkins[3], L. Norman[2], O. Flanagan[1], S. Rynders[3], B. I. Barton[3], R. N. C. Sanders[4], M. P. Meredith[4], C. Arrowsmith[5], and M. C. Lohan[1]

[1]School of Ocean and Earth Science, University of Southampton, Southampton, UK, [2]School of Environmental Sciences, University of Liverpool, Liverpool, UK, [3]National Oceanography Centre, Liverpool, UK, [4]British Antarctic Survey, Cambridge, UK, [5]British Geological Survey, Keyworth, UK

Abstract Dissolved iron (dFe) and manganese (dMn) are essential micronutrients required in marine primary production; however, their low availability limits productivity and impacts the efficiency of the biological carbon pump. Therefore, it is crucial to elucidate their sources, sinks, and internal cycling. We present high-resolution dFe and dMn measurements from the Barents Sea during summer 2023, to provide new insights into their spatial distribution and biogeochemical cycling. Localized surface enrichment of dFe and dMn indicate inputs from sea ice (Fe: 0.23–1.31 and Mn: 3.55–7.33 nmol/kg) and glacial melt (Fe: 1.17–3.19 and Mn: 22.44–102 nmol/kg). In the subsurface waters, dFe and dMn maxima (Fe: 4.95–10.70 and Mn: 9.05–33.61 nmol/kg) are a result of sediment resuspension, indicated by low beam transmission. Using the spatial distribution of dFe and dMn and their correlation with salinity and seawater isotopic composition, these inputs were found to be spatially constrained, with limited vertical and lateral transport from the source regions. We observed high rates of primary productivity in the upper 51 m of the southwestern Barents Sea (2,200 ± 222 mg C m^{-2} d^{-1}), corresponding to depleted dFe and dMn in the surface waters (Fe: 0.08–0.18 and Mn: 0.18–3.15 nmol/kg). Using nutrient limitation ratios, we found potential Fe-limitation in the southern Barents Sea, resulting from limited vertical resupply of Fe and high biological uptake. Our results suggest that Atlantification is causing the southwestern Barents sea to transition to an Atlantic-like seasonally Fe-limited system.

Plain Language Summary Marine phytoplankton growth influences climate and ecosystems but depends on the availability of iron and manganese in the ocean. These nutrients are found at very low concentrations and can limit phytoplankton growth. Understanding where iron and manganese come from (sources), how they are removed (sinks), and how they are cycled while in the ocean is important. The Barents Sea is one of the most productive regions in the Arctic, but it is rapidly warming. We measured iron and manganese in the Barents Sea to better understand their cycling and impact on marine phytoplankton. We found that sea ice and glacial melt provide iron and manganese to the surface of the Barents Sea and sediment resuspended from the seafloor provides them close to the seabed. However, these inputs do not spread far from their sources. In the southwestern Barents Sea, phytoplankton used much of the available iron and manganese, and iron supply was very limited, resulting in very low surface concentrations. As the Barents Sea warms, rising demand and falling supply of iron and manganese could spread iron limitation, affecting future phytoplankton growth.

Key Points:

- Sea ice, glacial melt, and sediment resuspension are the main inputs of dissolved iron and manganese to the Barents Sea
- High productivity depletes iron and manganese from the surface waters of the southwestern Barents Sea
- As the Barents Sea shifts from an Arctic to an Atlantic system due to Atlantification, it may become seasonally iron and nitrate co-limited

Supporting Information:

Supporting Information may be found in the online version of this article.

Correspondence to:

M. C. Lohan,
M.Lohan@soton.ac.uk

Citation:

Hawley, R., Mahaffey, C., Hopkins, J., Norman, L., Flanagan, O., Rynders, S., et al. (2026). Iron and manganese cycling in the atlantifying Barents Sea: Concentrated inputs and emerging limitations. *Global Biogeochemical Cycles*, *40*, e2025GB009031. https://doi.org/10.1029/2025GB009031

Received 17 DEC 2025
Accepted 6 APR 2026

Author Contributions:

Conceptualization: R. Hawley, C. Mahaffey, J. Hopkins, M. C. Lohan
Data curation: R. Hawley, J. Hopkins, S. Rynders, B. I. Barton
Formal analysis: R. Hawley, C. Mahaffey, J. Hopkins, R. N. C. Sanders, M. P. Meredith, M. C. Lohan
Funding acquisition: C. Mahaffey, J. Hopkins, M. C. Lohan
Investigation: R. Hawley, C. Mahaffey, J. Hopkins, L. Norman, O. Flanagan, S. Rynders, B. I. Barton, R. N. C. Sanders, M. P. Meredith, C. Arrowsmith, M. C. Lohan
Project administration: C. Mahaffey, J. Hopkins, M. C. Lohan

1. Introduction

Primary productivity by phytoplankton in the oceans is responsible for about half of all carbon fixation associated with global primary production (Field et al., 1998). Iron (Fe) and manganese (Mn) are essential micronutrients for marine primary productivity and are required for key phytoplankton metabolic functions (Morel & Price, 2003; Twining & Baines, 2013). Their redox chemistry makes these elements well suited for electron transport reactions in processes such as photosynthesis and respiration (Raven, 1988; Raven et al., 1999). However, dissolved Fe (dFe; <0.2 μm) is present at nano- to sub-nanomolar concentrations over large regions of the ocean, limiting primary production across approximately one-third of the global ocean (Martin, 1990; J. K. Moore et al., 2001). This reduces the efficiency of the biological carbon pump, which drives the drawdown of atmospheric CO_2 and plays a key role in regulating the global climate (Martin, 1990; C. M. Moore et al., 2013). Dissolved Mn (dMn; <0.2 μm) is also present at nanomolar concentrations in the ocean, yet dMn is often enriched in surface waters due

Resources: R. Hawley, C. Mahaffey, J. Hopkins, M. C. Lohan
Supervision: M. C. Lohan
Validation: R. Hawley, M. C. Lohan
Visualization: R. Hawley
Writing – original draft: R. Hawley
Writing – review & editing: R. Hawley, C. Mahaffey, J. Hopkins, L. Norman, O. Flanagan, S. Rynders, B. I. Barton, R. N. C. Sanders, M. P. Meredith, C. Arrowsmith, M. C. Lohan

to the photoreduction of Mn(III/IV) oxides (MnOx) and maintained by the photoinhibition of microbially mediated Mn(II) oxidation to MnOx (Sunda & Huntsman, 1994). Consequently, Mn is not typically found at limiting concentrations in the surface ocean (Hatta et al., 2015; Landing & Bruland, 1987), with the exception of the Drake Passage and Southeast Pacific (Browning et al., 2021; Hawco et al., 2022; M. Wu et al., 2019). However, Mn cycling influences other biogeochemical processes and can provide valuable insights into the cycling of other trace elements, including Fe. Together, these key micronutrients play a fundamental role in global ocean biogeochemical cycling (Boyd & Ellwood, 2010; Bruland et al., 1991; Morel & Price, 2003; Tagliabue et al., 2017).

Both Fe and Mn share common sources, such as shelf sediments (Froelich et al., 1979; Johnson et al., 1999; J. K. Moore & Braucher, 2008), sea ice (Grotti et al., 2005; Lannuzel et al., 2007; Tovar-Sánchez et al., 2010), glacial meltwater (Hawkings et al., 2020; Raiswell et al., 2006; Wehrmann et al., 2014), aeolian dust deposition (Jickells, 1995), riverine runoff (de Baar & de Jong, 2001; Guieu et al., 1996), and hydrothermal vents (Elderfield & Schultz, 1996). Similar removal processes, include oxidative precipitation (Bruland & Lohan, 2003), scavenging (Bruland & Lohan, 2003; J. Wu et al., 2001), and biological uptake (Bruland et al., 1991; Sunda, 2012), though the biological uptake stoichiometry varies significantly between Fe and Mn (Twining & Baines, 2013). The similarities in the biogeochemical cycling of Fe and Mn enable comparisons of their fluxes and distributions, particularly in shelf environments where their coupled enrichment can be used as indicators of a common source flux (Colombo et al., 2020; Hatta et al., 2015; Jensen et al., 2020; Landing & Bruland, 1987; Sedwick et al., 2000). Comparative analysis of Fe and Mn is a powerful approach for identifying dominant sources, constraining removal processes, and understanding trace element behavior in dynamic shelf and slope environments. Despite their similar external sources, the relative contributions and chemical speciation of these sources, coupled with the differing reactivity of these elements, can result in changes in the Fe/Mn stoichiometry in the ocean, causing Fe and Mn cycling to become uncoupled (Jensen et al., 2020).

The Arctic Ocean is a complex environment dominated by shallow continental shelves (>50% by area) (Jakobsson, 2002). The interplay between sea ice dynamics, riverine and glacial discharge, and shelf-basin exchange creates marked spatial and temporal variability, resulting in generally high concentrations of dissolved Fe and Mn in the Arctic Ocean and its surrounding shelf seas (Colombo et al., 2020, 2021; Jensen et al., 2020; Kanna et al., 2025; Klunder, Bauch, et al., 2012; Klunder, Laan, et al., 2012; Rijkenberg et al., 2018). Studies have previously focussed primarily on the Nansen and Amundsen Basins (Klunder, Bauch, et al., 2012; Klunder, Laan, et al., 2012; Middag et al., 2011; Rijkenberg et al., 2018), the Canadian Basin and adjacent Chukchi Shelf (Aguilar-Islas et al., 2013; Jensen et al., 2020; Kondo et al., 2016), and the Laptev and East Siberian Seas (Kanna et al., 2025). Comparatively, Fe and Mn biogeochemistry in the Barents Sea has received little attention (Gerringa et al., 2021). As one of the most biologically productive sectors of the Arctic Ocean (Carmack & Wassmann, 2006; Sakshaug, 1997; Sakshaug & Slagstad, 1991), the Barents Sea plays a disproportionate role in regional carbon exports, making it a critical region for understanding Fe and Mn dynamics.

In recent decades, the Arctic has been warming up to four times faster than the global average (Rantanen et al., 2022). Concurrently, the advection of warm sub-Arctic Atlantic-origin water into the Arctic Ocean, Atlantification, has been warming and weakening the stratification of the Barents Sea and proceeding further into the Eurasian Basin (Lind et al., 2018; Polyakov et al., 2017, 2025). This has been accompanied by a 9% decline in sea ice concentration per decade (Comiso, 2012), substantial melt of glaciers on the Svalbard archipelago (mass loss rate of 7 ± 4 Gt yr^{-1} during 2000–2019 van Pelt & Frank, 2025), and an 88% increase in primary production in the Barents Sea, at a rate of 3.73 Tg C $year^{-1}$ (Arrigo & van Dijken, 2015; Arrigo et al., 2008; Lewis et al., 2020). This transition from an Arctic to an Atlantic system is likely to alter the micronutrient biogeochemistry of the Barents Sea, highlighting the need for improved understanding of Fe and Mn cycling in this system.

Here, we present concentrations of dFe and dMn from a high-resolution surface transect and depth profiles, alongside other biogeochemical components, to (a) investigate the distribution of Fe and Mn in the Barents Sea, (b) elucidate the mechanisms controlling the spatial distributions of these trace elements, and (c) assess the potential influence of Fe and Mn on phytoplankton productivity, in the Barents Sea. This study provides new insights into trace element cycling in a rapidly changing Arctic shelf sea.

10.1029/2025GB009031

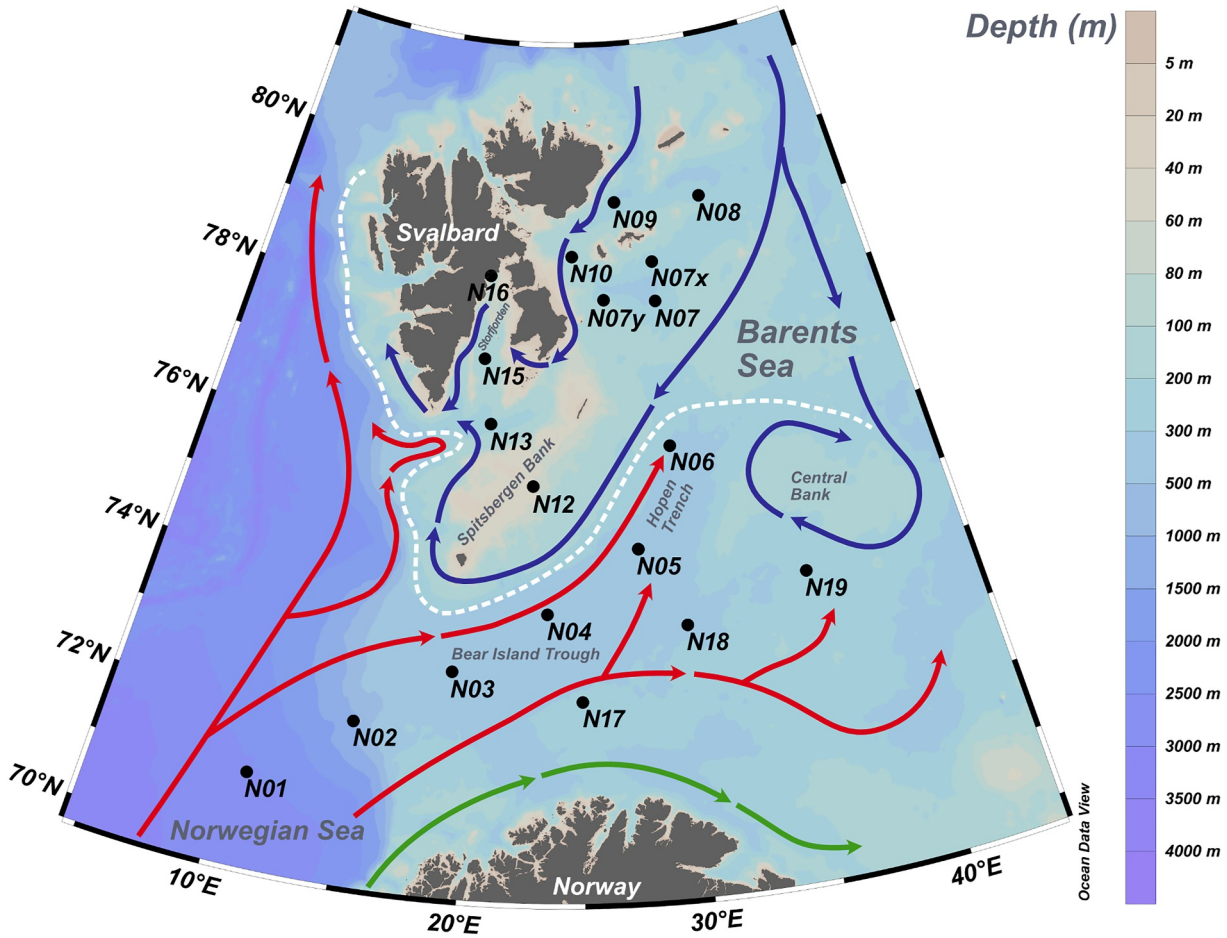

Figure 1. Bathymetric map of the Barents Sea, with locations of stations sampled during DY167 (black dots and numbers). The general circulation of water masses is shown as solid arrows, with Atlantic Water in red, Arctic Water in blue, and the Norwegian Coastal Current in green. The dashed white line represents the approximate location of the Polar Front. The seafloor depth is shown by the background color, with major bathymetric features labeled in gray.

2. Study Site

The Barents Sea is a shallow Arctic shelf sea (Figure 1), with an average depth of 230 m, occupying approximately 10% of the Arctic Ocean's surface area (Loeng, 1991). Despite its limited volume, the Barents Sea acts as a transition zone between the temperate and sub-polar North Atlantic and the Arctic Ocean (Smedsrud et al., 2013). The southwestern Barents Sea is a gateway for warm and saline Atlantic Water (AW) entering the Arctic Ocean (Loeng, 1991), with a net inflow of ~2 Sv through the Barents Sea Opening (Barton et al., 2018; Skagseth, 2008). Conversely, in the northern Barents Sea there is an influx of cold Arctic Water (ArW) from the central Arctic Ocean through the opening between Svalbard and Frans Josef Land (Loeng, 1991), along with seasonal sea ice import (Lind et al., 2016). The convergence of these water masses is marked by the Barents Sea Polar Front (Figure 1) (Barton et al., 2020; Loeng, 1991; Oziel et al., 2016). The Polar Front is a key site for water mass transformation with a significant influence on local biogeochemistry (Årthun et al., 2012). The Barents Sea has complex topography, characterized by shallow banks (~50 m) and deep channels and troughs (up to 500 m), driving intricate circulation patterns. There is also a large (~190 km long) and deep (~190 m) fjord, Storfjorden, located along the southeastern coast of Svalbard, which is separated from the Barents Sea by a 120 m-deep sill at 77°N (Vivier et al., 2023) (Figure 1).

3. Materials and Methods

3.1. Sample Collection

Seawater samples were collected from the Barents Sea in summer 2023 (9 July–12 August), onboard the *RRS Discovery* (DY167) (Figure 1). Seawater samples were collected using a titanium rosette fitted with 24 × 10 L trace metal-clean Teflon-coated Ocean Test Equipment (OTE) bottles and CTD profiler (Sea-Bird Scientific) deployed on a conducting Kevlar wire. Upon recovery, the OTE bottles were transferred to the shipboard class-1000 clean laboratory and pressurized (0.6 bar) with compressed air filtered in-line through a 0.2 µm PTFE filter (Millex-FG 50, Millipore). Subsamples for dissolved trace metals (dTM) were filtered through a 0.2 µm membrane filter (Sartobran 300, Sartious) into 125 mL trace metal-clean low density polyethene (LDPE) bottles and acidified to pH 1.7 (0.024 M) by addition of 12 M HCl (Romil, UpA) (Lohan et al., 2006). The surface samples were collected every two hours by a towed "fish" sampler and pumped into the clean laboratory using a Teflon diaphragm pump (A-15, Almatec) connected by acid-washed PVC tubing. The dTM samples were filtered in-line and acidified following the same procedure as above.

3.2. Trace Metal Analyses

Two analytical methods were conducted. Samples for dFe were analyzed using flow injection analysis with chemiluminescence detection (Kunde et al., 2019) inside a class-1000 clean air laboratory onboard the *RRS Discovery*. The limit of detection (3σ of the analytical blank) was 0.03 ± 0.01 nmol/kg (n = 21). Accuracy was established by repeat quantification of dFe in an internal reference standard (ZIPLOC II; 0.29 ± 0.05 nM), yielding an average concentration of 0.24 ± 0.03 nmol/kg (n = 15), which agrees with the consensus value. Samples for dFe and dMn were analyzed using offline pre-concentration and extraction following the manifold design by Milne et al. (2010) and the extraction chemistry by Rapp et al. (2017), followed by ICP-MS detection, at the University of Southampton, UK. The limit of detection was 0.07 ± 0.03 nmol/kg for Fe and 0.09 ± 0.02 nmol/kg for Mn (n = 45). Accuracy was established by repeat quantification of GEOTRACES reference standards (Table S1 in Supporting Information S1). Methods for the measurement of the auxiliary parameters are described in Text S1, Table S2 in Supporting Information S1.

4. Results and Discussion

4.1. Hydrography

Water masses were identified from samples collected during this study using optimum multiparameter analysis (Ilyas et al., 2026). Five principal water masses were identified: Atlantic Water (AW), warm Atlantic Water (wAW), Arctic Water (ArW), warm Arctic Water (wArW), and Glacial Water (GW) (Figure 2).

Strong north-south hydrographic gradients were observed in the Barents Sea, shaped by the inflow of AW from the south and ArW from the north, with localized mixing over topographic features. The Polar Front marked the sharp transition between these water masses, at ~76°N (Figure 2). South of the Polar Front, wAW dominated the surface layer (<50 m), with AW comprising the underlying the water column (Figure 2a). North of the Polar Front, the surface layer (<50 m) was characterized by wArW, underlain by ArW in the subsurface water column (Figure 2a).

Within the Barents Sea, shallow banks and topographic features are sites of elevated tidal mixing and reduced stratification. Over the Spitsbergen Bank (Station N12), the water column was well mixed, likely due to tidal and wind-driven mixing (Fer & Drinkwater, 2014) and contained nearly equal mixtures of wAW, ArW, and GW (Figure 2c). North of the Spitsbergen Bank, the water within the Storfjordrenna Trough (Station N13) is predominantly AW, as a result of topographically steered inflow from the West Spitsbergen Current.

In the Storfjorden system along the eastern coast of Svalbard (Station N15 and N16), ArW was the dominant water mass below ~50 m, consistent with Vivier et al. (2023) (Figure 2c). The upper 30 m of the water column contained a high fraction of wAW, which was likely advected into the fjord by wind and currents, and mixed with ArW. The surface water (<5 m) adjacent to the glacier terminus (Station N16) was dominated by a glacial surface plume, varying between 50% and 100% GW over the sampling period. The GW content of the surface water remained high 50 km south of the glacier terminus in Storfjorden but had declined substantially by Station N15 (<40% GW), with only a 0%–10% GW contribution in surface waters past the Storfjorden sill.

10.1029/2025GB009031

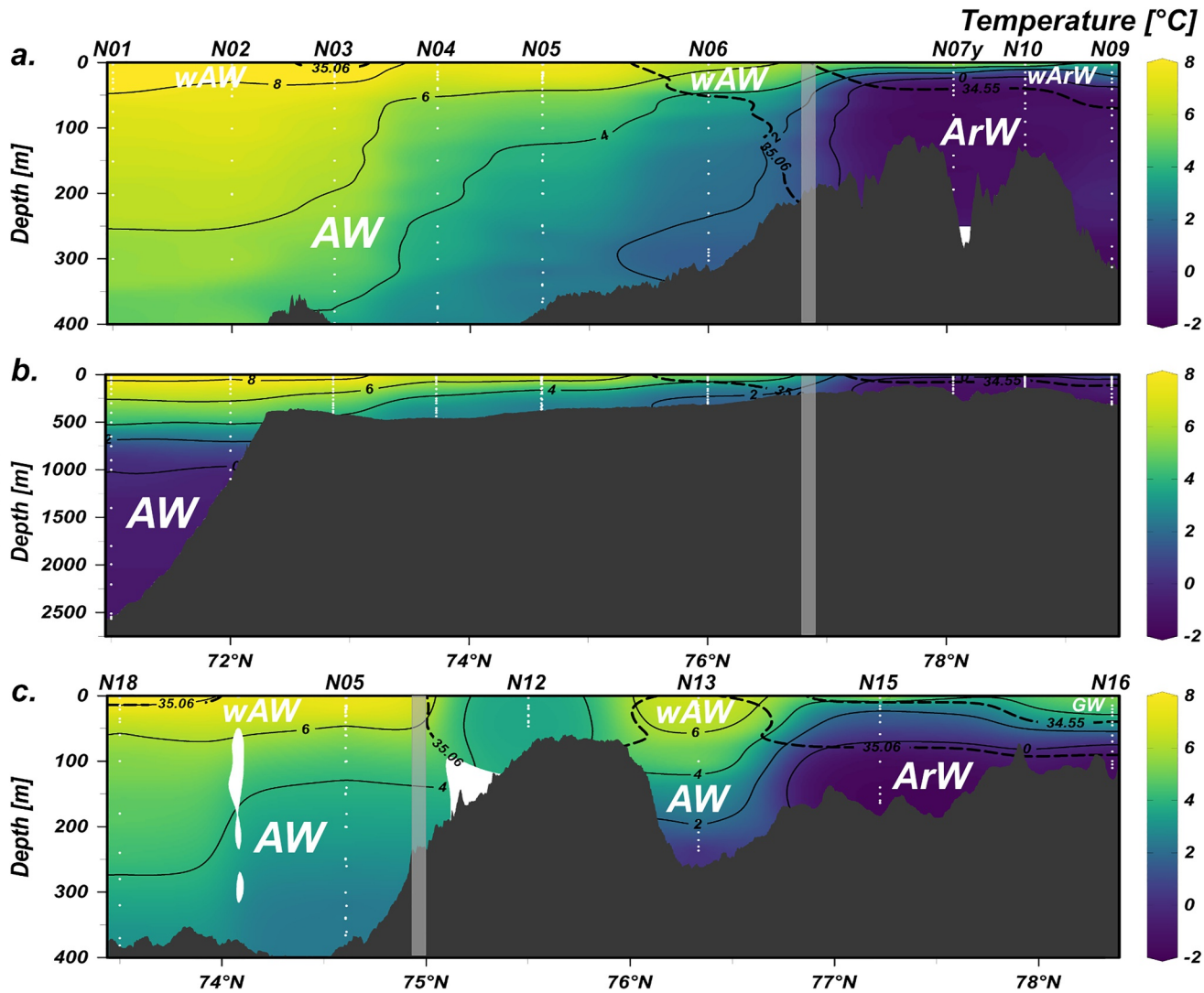

Figure 2. Section plots of conservative temperature against latitude from south to north along (a) Transect 1 (upper 400 m), (b) Transect 1 (full depth), and (c) Transect 2 (full depth). Station numbers are labeled in black above the transects. See Figure 1 for the location of stations in each transect. White dots show the sampled depths. Solid black lines represent temperature contours and dashed black lines represent salinity contours. Atlantic Water (AW), warm Atlantic Water (wAW), Arctic Water (ArW), warm Arctic Water (wArW), and Glacial Water (GW) are labeled in white. The approximate location of the Polar Front is denoted by a gray bar.

4.2. Spatial Variability of Dissolved Fe and Mn in the Barents Sea

Concentrations of dFe and dMn varied by more than two orders of magnitude (Figures 3–5). This wide range in concentrations demonstrates the strong spatial heterogeneity in the sources and cycling of these trace elements in a dynamic shelf system and is consistent with the limited number of previously published trace element measurements in the Barents Sea (Klunder, Bauch, et al., 2012; Klunder, Laan, et al., 2012; Rijkenberg et al., 2018).

Concentrations of dFe and dMn in the surface waters of the Barents Sea ranged from 0.04–25.69 to 0.18–102.24 nmol/kg, respectively (Figure 3). Dissolved Fe and Mn exhibit similar spatial distributions, with the lowest concentrations observed south of the Polar Front in AW (0.04–0.89 and 0.18–4.12 nmol/kg, respectively), and higher variability north of the Polar Front (0.12–25.69 and 1.13–102.24 nmol/kg, respectively) in wArW. Three distinct surface hotspots of elevated dFe and dMn were identified. Intermediate concentrations of dFe and dMn were observed at the sea ice edge (78°N to 79.41°N), ranging from 0.23–1.31 to 3.55–7.33 nmol/kg, respectively. Elevated concentrations of dFe (3.26–25.69 nmol/kg) and dMn (8.36–15.51 nmol/kg) were observed on the Spitsbergen Bank. The most pronounced surface enrichment was found within Storfjorden, where

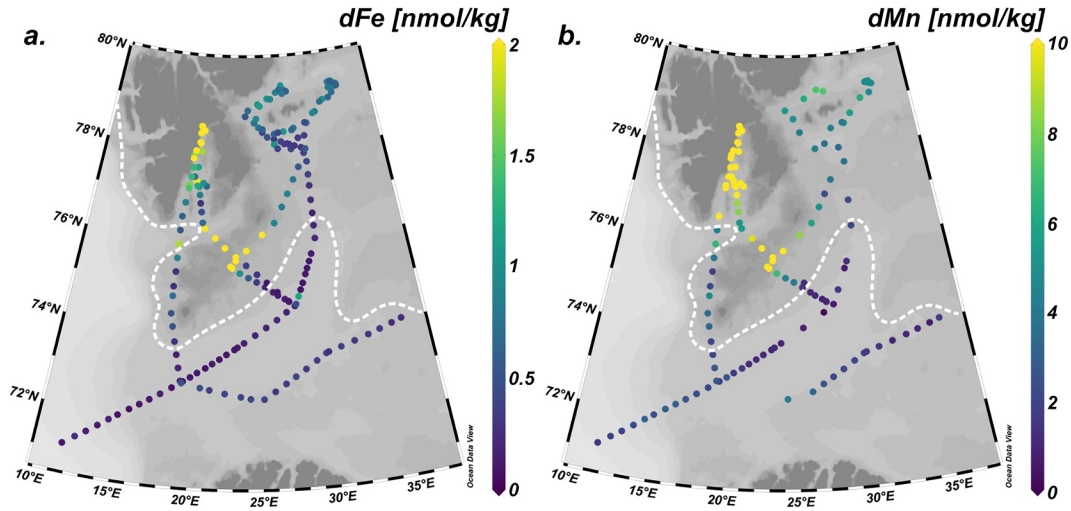

Figure 3. Surface plots of (a) dFe and (b) dMn in the Barents Sea, with a color bar to show concentration. The approximate location of the Polar Front is denoted by a white dashed line.

dFe (1.17–3.19 nmol/kg) and dMn (22.44–102.25 nmol/kg) surface concentrations peaked adjacent to a marine-terminating glacier.

The spatial patterns of dFe and dMn seen at the surface are also found through the water column, with lower concentrations south of the Polar Front (dFe: 0.07–0.68 nmol/kg; dMn: 0.99–2.25 nmol/kg) and higher variability values to the north (dFe: 0.32–4.08 nmol/kg; dMn: 1.55–4.09 nmol/kg) in the upper 100 m (Figures 4 and 5). Although spatially variable, the vertical distributions of dFe and dMn in the Barents Sea displayed a similar shape, with lower concentrations in the upper water column (dFe: 0.07–4.08 nmol/kg; dMn: 0.99–4.84 nmol/kg), increasing with depth and peaking in the bottom waters (dFe: 0.89–10.71 nmol/kg; dMn: 0.29–33.61 nmol/kg) (Figures 4 and 5). Notably, concentrations of dFe and dMn were higher in the bottom waters on the shallow shelf (dFe: 1.05–10.71 nmol/kg; dMn: 1.00–33.61) compared to the deep Norwegian Basin (Station N01, dFe: 0.89 nmol/kg; dMn: 0.30 nmol/kg) and the shelf slope (Station N02, dFe: 1.02 nmol/kg; dMn: 0.58 nmol/kg) (Figure 4). On the Spitsbergen Bank (Station N12), dFe and dMn concentrations were elevated throughout the entire water column, ranging from 6.65–13.27 to 13.25–16.22 nmol/kg, respectively (Figure 5). In Storfjorden, vertical concentrations of dFe and dMn were consistently high at the station closest to the glacier terminus, Station N16 (dFe: 1.87–2.84 nmol/kg; dMn: 29.28–189.20 nmol/kg) (Figure 5). Away from the glacier (Station N15), dFe and dMn concentrations decreased but remained elevated (dFe: 1.32–2.60 nmol/kg; dMn: 1.75–15.70 nmol/kg), relative to waters outside the fjord. The spatial distribution of dFe and dMn reflects the complex interplay of inputs, transport and biological uptake in controlling the biogeochemical cycling of these trace elements in the Barents Sea.

4.3. Sedimentary Inputs

The highest concentrations of dFe and dMn in the water column were typically found in the bottom waters of the Barents Sea shelf (dFe: 0.89–10.71 nmol/kg; dMn: 0.29–33.61 nmol/kg) (Figures 4a, 4b, 5a, and 5b), suggesting that shelf sediments are a significant source. Sedimentary inputs have been found to be a large source of trace elements in other Arctic shelf seas, with evidence of their lateral transport into the central Arctic Basin (Colombo et al., 2020, 2021; Klunder, Laan, et al., 2012).

These inputs can occur from the resuspension of sediments and/or from the reductive-dissolution of solid phases during porewater diagenesis. To distinguish sediment resuspension from pore water diagenetic fluxes, we employed the quasi-conservative tracer N^* ($N^* = 0.87 \times ([NO_3^-] - 16[PO_4^{3-}])$ μmol/L; Gruber & Sarmiento, 1997), where strongly negative values indicate denitrification and reducing conditions within sediments. N^* is an ideal tracer of porewater diagenesis in this region, as water column denitrification in the Barents Sea is unlikely due to high water column oxygen concentrations. Thus, the low N^* values are attributed to processes occurring within porewaters. Dissolved Fe and Mn concentrations from the deepest samples exhibit a strong

10.1029/2025GB009031

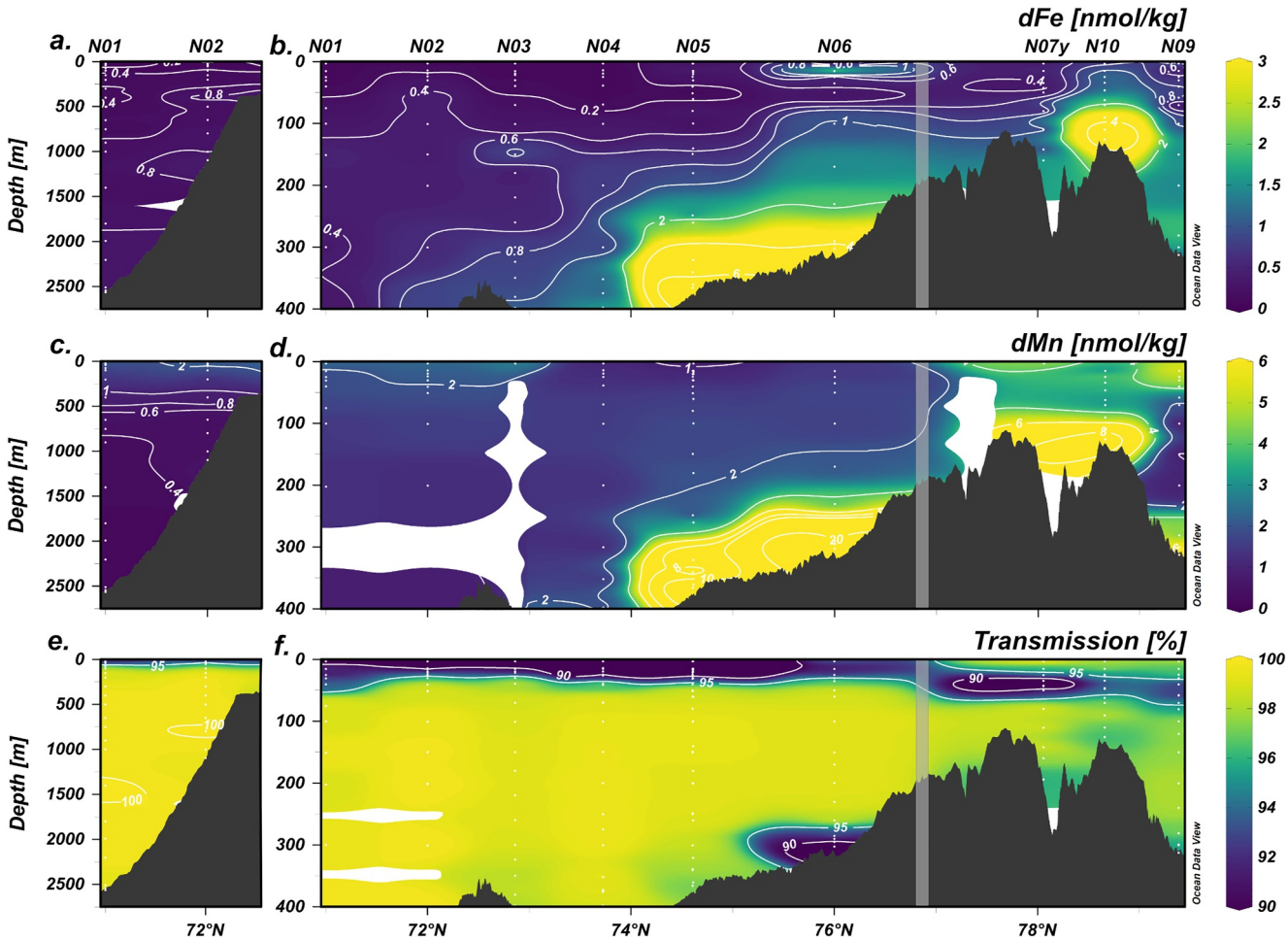

Figure 4. Section plots of (a, b) dFe, (c, d) dMn, and (e, f) beam transmission against latitude along Transect 1. Panels (a), (c), and (e) show full-depth profiles at Stations N01 (off-slope) and N02 (slope). Panels (b), (d), and (f) show the upper 400 m along the full transect (Stations N01–N09), to highlight the-to-basin gradient. Station number is indicated at the top of the plot. Each pair of plots shares the same color bar. White dots show sample depths at each station. The approximate location of the Polar Front is denoted by a gray bar. White contours indicate equidistant concentrations in plots (a)–(d). White contours indicate equidistant transmission intervals in plots (e) and (f).

inverse relationship with N^* (dFe: $r = -0.70$, $r^2 = 0.49$, $p = 0.004$; dMn: $r = -0.86$, $r^2 = 0.74$, $p = 4.0 \times 10^{-5}$), with negative values of N* (−0.74 to −2.97 μmol/L) found at all locations (Figure 6), indicating the presence of a diagenetic porewater source. However, in stronger reducing conditions in the Arctic Ocean, N^* was more negative, such as through the Bering Strait and on the eastern Chukchi Shelf, where N^* was as high as −15 (Colombo et al., 2020, 2022; Jensen et al., 2020; Kanna et al., 2025). Investigations of sediment mixing and oxygen penetration depth of Barents Sea surface sediments show that at least the top 1 cm is homogenized through biological and/or physical mixing, and the oxygen penetration depth is >1 cm in most locations (Faust et al., 2020), making strongly reducing conditions in the upper sediment porewaters unlikely to occur. These results suggest that while porewater diagenesis contributes to elevated Fe and Mn concentrations, it is not the dominant source. Instead, desorption/dissolution during sediment resuspension appears to be the primary source of dFe and dMn in the bottom waters of the Barents Sea. Our transects pass across Spitsbergen Bank (Station N12), which has been found to have near-bottom mixing, driven mainly by strong near-bottom currents induced by tidal stirring together with tidal straining interacting with the complex topography of the Barents Sea (Fer & Drinkwater, 2014). The strong density gradients across the Spitsbergen Bank Polar Front have been found to produce a south-westward along-front jet (0.1–0.2 m s^{-1}) between the 150 and 250 m isobaths that would tend to advect resuspended sediments along the slope of the bank around N6 and N12 (Våge et al., 2014), acting as a source of dFe and dMn.

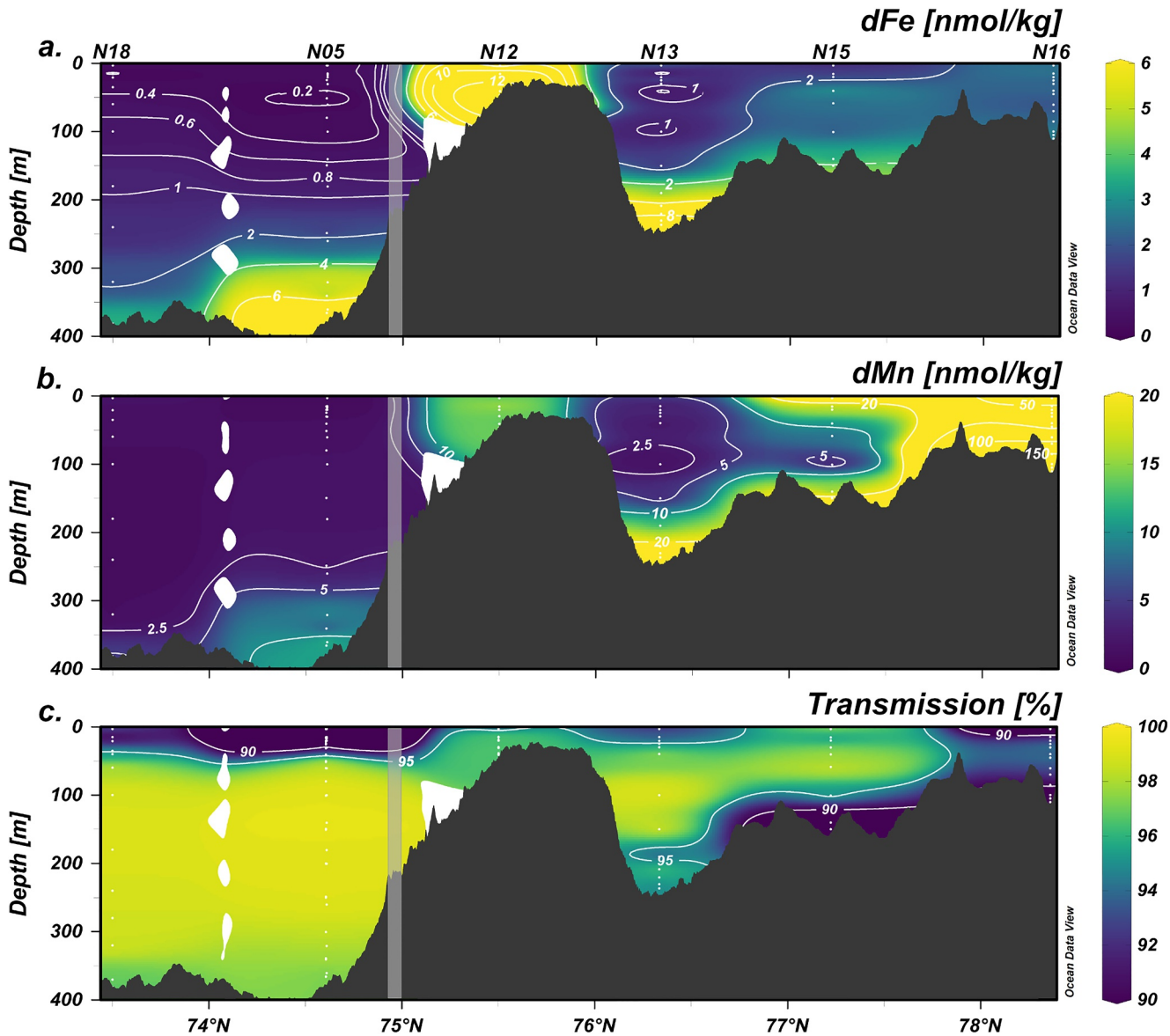

Figure 5. Section plots of (a) dFe, (b) dMn, and (c) transmission against latitude along Transect 2 (full depth). Station number is indicated at the top of the plot. White dots show sample depth at each station. The approximate location of the Polar Front is denoted by a gray bar. White contours indicate equidistant concentrations in plots (a) and (b). White contours indicate equidistant transmission intervals in plot (c).

While both dFe and dMn were enriched in the bottom waters of the Barents Sea from porewater diagenesis and sediment resuspension fluxes, dMn concentrations were significantly higher than dFe at almost all locations. This is likely because dFe is rapidly oxidized and reprecipitated as insoluble Fe(III) in the presence of oxygen, with a half-life on the order of minutes, even in cold seawater (Jensen et al., 2020; Millero et al., 1987; Sarthou et al., 2011). Conversely, dMn oxidizes much more slowly in the presence of oxygen (von Langen et al., 1997; Yeats & Strain, 1990), with oxidation occurring over days to weeks in seawater (Jensen et al., 2020).

Sediment enrichment of dFe and dMn decrease from the shelf to the deep basin along Transect 1 (Stations N05, N04, N03 on the shelf; N02 on the slope; N01 off-slope). On the shelf, bottom water concentrations were higher (dFe: 1.05–11.44 nmol/kg; dMn: 1.00–33.61 nmol/kg), with enrichment extending tens of meters into the water column, whereas dFe and dMn on the shelf slope (dFe: 1.02 nmol/kg; dMn: 0.58 nmol/kg) and off-shelf (dFe: 0.89 nmol/kg; dMn: 0.30 nmol/kg) were lower, with enrichment observed near sediments only. This contrast highlights the importance of sedimentary sources on the shallow shelf, where sediment resuspension and

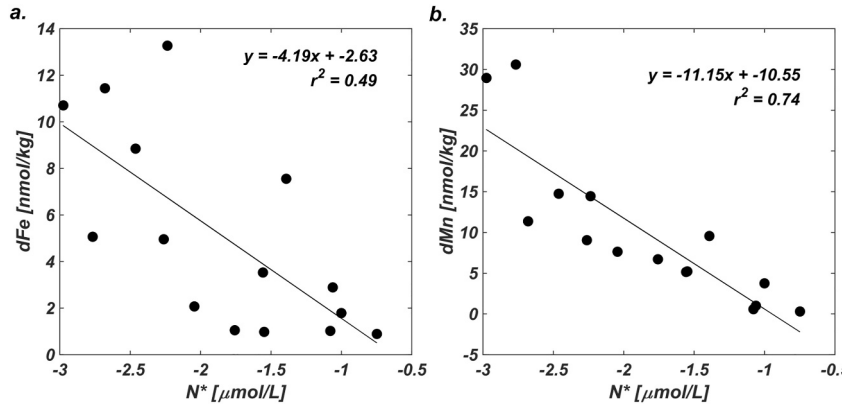

Figure 6. Scatter plots of (a) dFe and (b) dMn against N^* values from the deepest sample at every station. The deepest sample was within 5 m of the seafloor at every station; this was determined by the CTD altimeter sensor. The solid line shows the linear regression fit, with the regression equation and coefficient of determination (r^2) displayed on the plot.

diagenetic-release contribute to the inventories of dFe and dMn. However, even on the shelf, enrichment of dFe and dMn is restricted to deeper waters (>250 m) (Figures 4 and 5), indicating limited vertical transport. Only at a shallow bank station (N12; depth ∼50 m) do these sedimentary inputs of Fe and Mn extend to the surface. Tidal and wind-driven mixing is able to overcome the stratification induced by fresh melt water and solar heating (Fer & Drinkwater, 2014), resulting in sustained sediment resuspension and year-round vertical mixing.

4.4. Glacial Inputs

Glacial meltwaters are significant regional sources of dissolved trace elements to the polar oceans, with glacial Fe concentrations typically much higher than those in ambient seawater (Aciego et al., 2015; Bhatia et al., 2013; Jones et al., 2025). Although less is known about glacial Mn concentrations, elevated Mn concentrations in glacial meltwaters have also been reported in the Gulf of Alaska, with concentrations of 33–61 nmol/kg (Michael et al., 2023). In this study, the eastern coast of Svalbard is dominated by marine-terminating glaciers (Błaszczyk et al., 2009), providing a direct pathway for glacial meltwater to enter coastal waters. Accordingly, the concentrations of dFe and dMn are highly enriched in the surface waters (dFe: 1.17–3.19 nmol/kg; dMn: 22.44–102.25 nmol/kg) and throughout the water column (dFe: 1.87–2.85 nmol/kg; dMn: 29.28–189.20 nmol/kg) close to the glacier terminus in Storfjorden (Figure 3).

River runoff into the Barents Sea is very limited, with most rivers draining into isolated fjords instead (Faust et al., 2020), and the large outflows from the major Siberian and North American rivers exiting the Arctic via the west side of Fram Strait and the Canadian Arctic Archipelago. Consequently, the meteoric water fraction (f_{met}) measured from the $\delta^{18}O$ is interpreted as primarily reflecting glacial freshwater inputs, especially close to Svalbard. The surface samples, along the eastern coast of Svalbard (Figure S1 in Supporting Information S1), show a strong positive relationship between dFe, dMn and f_{met} (dFe: $r = 0.84$, $r^2 = 0.70$, $p = 3.1 \times 10^{-8}$; dMn: $r = 0.86$, $r^2 = 0.75$, $p = 3.0 \times 10^{-9}$; Figures 7a and 7b), indicating that runoff is a significant source of dFe and dMn to the surface of the Barents Sea in close proximity to glaciers.

The water column in close proximity (∼0.5 km) to the glacier (Station N16) shows clear enrichment of dFe and dMn (Figure 5). Marine terminating glaciers often discharge sediment-laden subglacial meltwater at depths of several hundred meters, which upwells along the calving front, entraining ambient fjord water, to form a buoyant plume, that may either reach the surface or achieve neutral buoyancy within the fjord subsurface before spreading laterally (Kanna et al., 2018, 2020; Mankoff et al., 2016; Motyka et al., 2013). The suspended particles within these plumes represent a dynamic, labile pool of trace elements which can act as either a source or sink of dissolved trace elements via reversible exchange, thereby buffering dissolved concentrations in the surrounding water column, depending on the ambient conditions (Annett et al., 2015; Lippiatt et al., 2010; Zhang et al., 2015). Concurrent with dFe and dMn enrichment, beam transmission was low (87%–95%) at Station N16. This negative correlation (dFe: $r = -0.84$, $p = 0.02$, $r^2 = 0.70$; dMn: $r = -0.95$, $p = 0.001$, $r^2 = 0.90$) demonstrates that

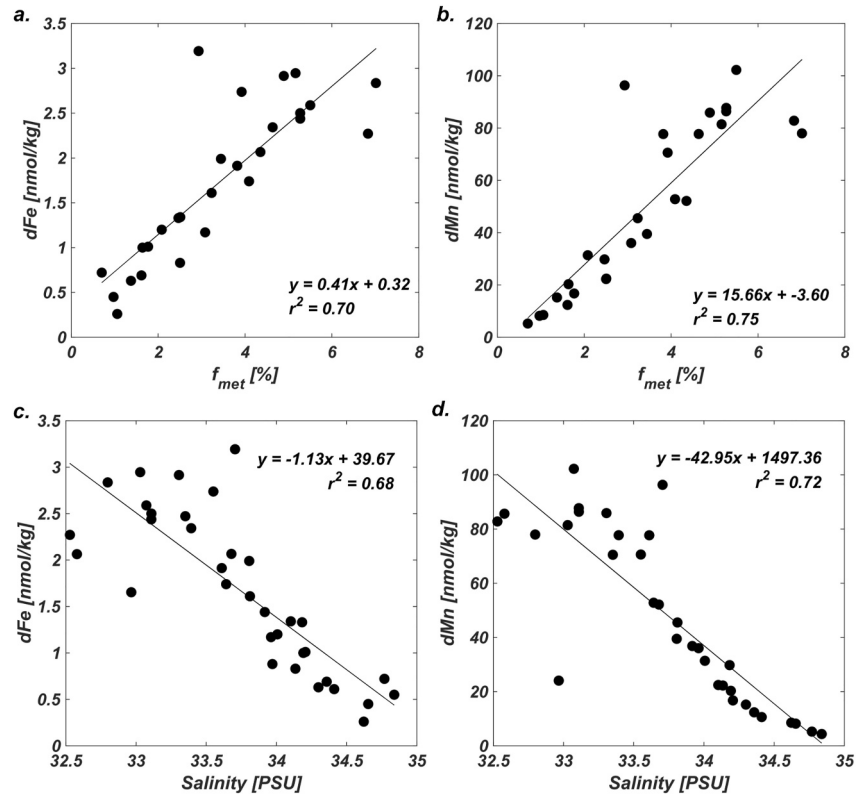

Figure 7. Scatter plots of (a) dFe and (b) dMn against the percentage of glacial melt (f_{met}), and (c) dFe, and (d) dMn against salinity for surface samples in Storfjorden. The solid line shows the linear regression fit, with the regression equation and coefficient of determination (r^2) displayed on the plot. For location of $\delta^{18}O$ surface samples see Figure S1 in Supporting Information S1.

subglacial discharge is a significant source of dissolved Fe and Mn in waters adjacent to marine-terminating glaciers in the Barents Sea.

Despite co-enrichment of Fe and Mn, dMn concentrations (22.44–189.20 nmol/kg) were consistently much higher than those of dFe (1.17–3.19 nmol/kg) at the surface and throughout the water column at the glacier terminus. These differences arise from the differing redox behavior and reactivity of Fe and Mn during the mixing of subglacial meltwater with oxygenated seawater (Zhu et al., 2024). Suspended particles within the subglacial discharge plume can continue to interact with the dissolved trace element pool through processes such as desorption, dissolution, scavenging, and precipitation (Jeandel & Oelkers, 2015; Jones et al., 2012, 2014; Michael et al., 2023; Pearce et al., 2013; Raiswell et al., 2016). These interactions are strongly influenced by water column conditions (e.g., salinity, temperature, pH, organic ligands) and by the mineralogy, surface area, and reactivity of the suspended particles (Boyd & Ellwood, 2010). Using dFe and dMn, in conjunction with the labile particulate (LpFe and LpMn) concentrations, we found that LpFe concentrations were substantially higher (11.65–39.69 nmol/kg), than dFe at Station N16 (Table S3 in Supporting Information S1), indicating that Fe was predominantly present as reactive Fe oxides, with dFe subject to rapid precipitation upon mixing with seawater (Millero et al., 1987). In contrast, LpMn concentrations (9.49–24.16 nmol/kg) were less than the dMn pool (Table S3 in Supporting Information S1), suggesting that Mn is predominantly present in the dissolved form as dMn is oxidized more slowly upon mixing with oxygenated seawater, resulting in an accumulation of dMn. Similar trends of excess dMn have been observed in situ in West Greenland (van Genuchten et al., 2022) and in incubation experiments with Arctic fjord sediments, which found that dMn increased and exceeded dFe concentrations within a few hours, despite much lower abundances of LpMn (Zhu et al., 2024).

While glacial meltwater contributes only a small fraction of dissolved Fe and Mn globally, it can represent an important source for regional Fe and Mn inventories (Hawkings et al., 2020; Kanna et al., 2020; Raiswell et al., 2006; Wehrmann et al., 2014). To assess the significance of these glacial inputs of dFe and dMn to the

Barents Sea inventory, we investigated the offshore transport of dFe and dMn away from their glacial inputs. Both dFe and dMn in the surface waters of the fjord exhibited similar distribution patterns of decreasing concentrations moving away from the glacier terminus (Figure 3). We observed a strong negative linear correlation between dFe ($r = -0.82$, $p = 2.4 \times 10^{-09}$, $r^2 = 0.68$), dMn ($r = -0.84$, $p = 4.5 \times 10^{10}$, $r^2 = 0.72$) and salinity (Figures 7c and 7d). Rapid coagulation and flocculation of dissolved Fe and Mn during estuarine mixing results in substantial removal at low salinities, as widely observed in estuaries and glacier systems, resulting in non-conservative macronutrient-salinity relationships (Hopwood et al., 2016, 2017; Kanna et al., 2020; Krause et al., 2021; Schroth et al., 2014; van Genuchten et al., 2021). Our results suggest that the exponential removal processes that occur at low salinity have already occurred upstream of the sampling site, closer to the glacier terminus, and the linear relationship observed in this study indicates that the distribution of the remaining dFe and dMn is controlled by the dilution of meteoric inputs of Fe and Mn. This process has not been observed in many other fjord systems (Shen et al., 2024). However, variability in the strength of this correlation with salinity indicates that dFe is more susceptible to non-conservative removal processes within the fjord, whereas dMn has greater retention within the surface waters due to photoreduction (Sunda & Huntsman, 1988) and its lower susceptibility to scavenging (Bruland & Lohan, 2003; Landing & Bruland, 1987).

At the fjord sill, surface water dFe (0.45 nmol/kg) declined back to ambient concentrations (defined here as the average dFe and dMn concentrations in surface wArW away from inputs; 0.42 ± 0.21 and 3.13 ± 1.13 nmol/kg, respectively). This suggests that glacially derived dFe was largely removed from surface waters before reaching the sill, via scavenging and biological uptake. In contrast, surface dMn concentrations at the fjord sill remained elevated (6.62 nmol/kg) relative to ambient values, consistent with the longer residence time of Mn in surface waters (Bruland et al., 1994; Landing & Bruland, 1987). Further evidence of minimal net export of dFe and dMn is observed deeper in the water column (Figure 5), where concentrations remain elevated away from the glacier (Station N15) but decline to ambient levels south of the sill (~77°N). While biogeochemical processes are likely the dominant mechanism for Fe and Mn removal within Storfjorden, the fjord sill may also act as a physical barrier, due to limited deep water export (Vivier et al., 2023), thus retaining or recirculating any remaining subsurface glacial inputs within the fjord. Meanwhile, surface waters enriched in Fe and Mn likely exit the fjord via the coastal current that curves westward around Svalbard toward the Fram Strait. However, this potential export in the surface current remains unclear, as no sampling was conducted along this potential export pathway.

4.5. Sea Ice Melt

The melting of seasonal sea ice results in the enrichment of dFe and dMn in high-latitude waters (Aguilar-Islas et al., 2008; Kanna et al., 2025; Lannuzel et al., 2007; Tovar-Sánchez et al., 2010). Previous studies have reported dFe of 2.92–376 nmol/kg (Aguilar-Islas et al., 2008) in Arctic sea ice, highlighting sea ice melt melting as a potentially significant source of dFe (Kanna et al., 2014; Measures, 1999; Tovar-Sánchez et al., 2010). Little is known about Mn in Arctic sea ice, though moderate concentrations of dMn have been observed therein (5.3 ± 3.3 nmol/kg; Kanna et al., 2025). During this study, dFe in the surface waters at the sea ice edge was highly variable (0.23–1.32 nmol/kg; Figure 3a), with some enrichment observed. Surface water dMn was enriched (3.43–7.33 nmol/kg; Figure 3b) at the ice edge, similar to the dMn sea ice endmember value reported by Kanna et al. (2025) in the Laptev Sea. The concentrations of dFe and dMn observed at the sea ice edge indicate localized inputs from melting sea ice during the sampling period, although this enrichment was not observed ubiquitously along the ice edge.

At the sea ice influenced stations (N08 and N09), we assessed the relationship between dFe and dMn concentrations, and the sea ice meltwater contribution (f_{sim}) (Figure 8), to determine the inputs from sea ice to the Barents Sea. The small fraction of sea ice meltwater present (<4%) does not show a clear correlation with the concentration of dFe ($r = -0.40$, $p = 0.18$, $r^2 = 0.16$) or dMn ($r = 0.30$, $p = 0.32$, $r^2 = 0.09$) (Figure 8). The poor correlations of dFe and dMn with f_{sim} through the water column, coupled with the patchy enrichment of dFe and dMn at the surface ice edge, is likely due to an interplay of dynamic processes. Samples were collected in August, after the onset of seasonal sea ice melt, and therefore did not capture the early stages of sea ice melt. Lannuzel et al. (2008) reported that approximately 70% of dFe within sea ice was released to the underlying surface seawater within the first 10 days of melt during a time-series experiment in the Weddell Sea pack ice. Additionally, in the northern Barents Sea, the spring blooms typically occur between April and July, coinciding with the time when sea ice melts (Lee et al., 2015). Thus, it is likely that much of the dFe and dMn within the sea ice was released to the surface seawater during the initial melt period, and these inputs were subsequently removed

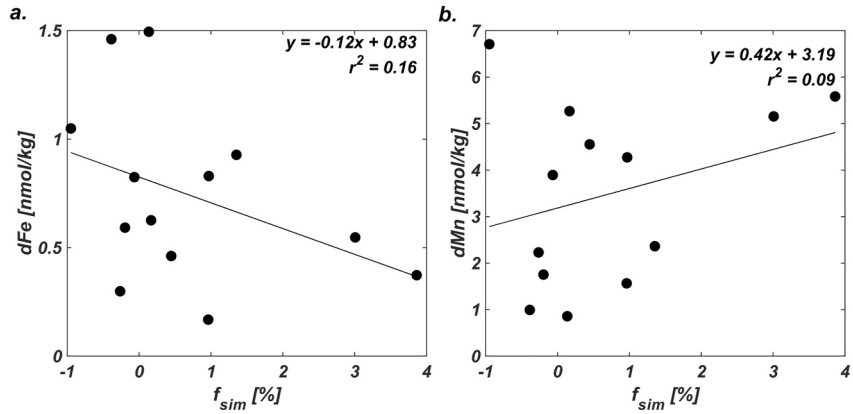

Figure 8. Scatter plots of (a) dFe and (b) dMn against the percentage of sea ice melt (f_{sim}) present at Stations N08 and N09. The solid line shows the linear regression fit, with the regression equation and coefficient of determination (r^2) displayed on the plot.

from the surface seawater through biological uptake and scavenging prior to sampling. Below the surface mixed layer, the bank (reaching 150 m isobath at station N10) enhances tidal current induced sediment resuspension, which provides an additional source of dFe and dMn to the water column below 50 m (Figure 4). Consequently, the elevated concentrations of dFe and dMn in the meltwater-influenced water column cannot be attributed solely to sea ice fluxes. Together, these observations suggest that sea ice meltwater was not a major contributor to the distributions of dFe and dMn in this region at the time of sampling, relative to other sources identified in this study, but may have been significant during the initial melt phase in spring.

The input of dFe and dMn from sea ice appears highly localized to the immediate ice edge (Figure 3). Elevated concentrations were confined to the northernmost surface samples (above 78.4°N). Away from the ice edge (77.2°N to 78.4°N), surface water concentrations of dFe and dMn are much lower (dFe: 0.26–0.63 nmol/kg; dMn: 3.43–4.41 nmol/kg), indicating that there is little lateral transport of dFe and dMn away from the ice edge.

4.6. The Role of Biological Uptake in the Spatial Distribution of Dissolved Fe and Mn

The Barents Sea is one of the most biologically productive shelf seas in the world's oceans, with an estimated average annual primary productivity of ∼100 g C m^{-2} $year^{-1}$ (Dalpadado et al., 2014; Reigstad et al., 2011). Given that dFe and dMn are essential for primary production (Bruland & Lohan, 2003; Morel & Price, 2003), biological uptake is likely a major control on the spatial distribution of these trace elements in the Barents Sea.

In the seasonally ice-covered northern Barents Sea, primary productivity was 1,227 ± 112 mg C m^{-2} d^{-1} integrated over the top 57 m across the Polar stations (Figure 1, stations north of the Polar Front), indicating that primary productivity is ongoing in the surface chlorophyll maximum, depleting residual sea ice melt-derived dFe and dMn. Thus, sea ice melt acts as a seasonal source of dFe and dMn to surface waters, creating a dynamic interplay between episodic trace element inputs and seasonal biological uptake.

In contrast, the AW-influenced southwestern Barents Sea had much higher rates of primary production (2,200 ± 222 mg C m^{-2} d^{-1} integrated over the top 51 m across stations south of the Polar Front), as primary production in this region accounts for ∼53% of total annual primary productivity in the Barents Sea (Arrigo & van Dijken, 2015; Castro de la Guardia et al., 2023). Correspondingly, dFe and dMn were significantly depleted in the surface ocean in this region (Figure 3). Dissolved Mn concentrations were not depleted to the same extent as dFe (Figure 3), as surface dMn is replenished through the photoreduction of Mn(III/IV) oxides (MnOx) and maintained by the photoinhibition of microbially mediated Mn(II) oxidation to MnOx (Sunda & Huntsman, 1988). Additionally, cellular demand for Mn in phytoplankton is lower (Raven et al., 1999). Thus, despite measurable dMn depletion, Mn-limitation is unlikely in this region. In contrast, dFe was severely depleted (0.08–0.18 nmol/kg). This indicates the potential for Fe-limitation on primary productivity occurring in the southwestern Barents Sea.

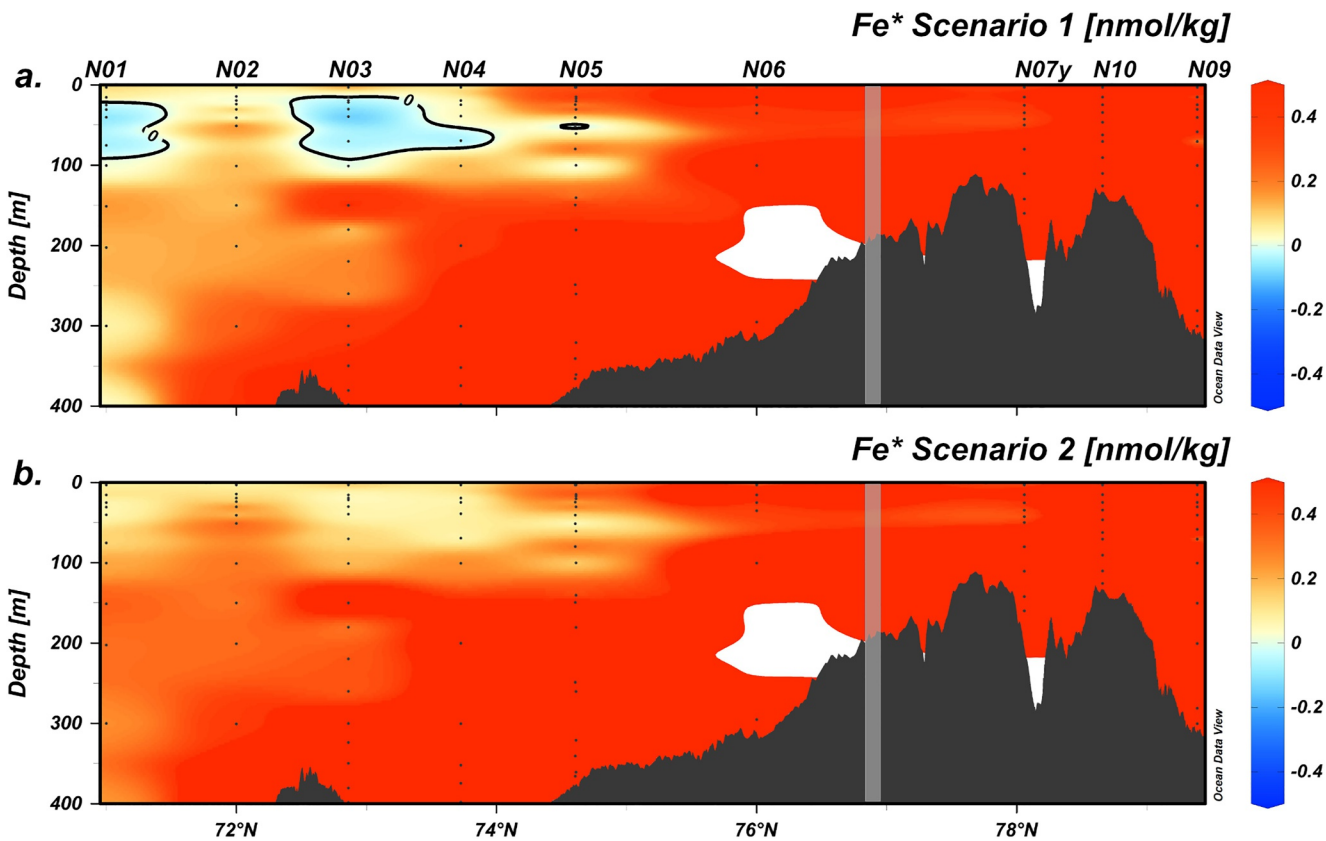

Figure 9. Section plot of Fe* under (a) scenario 1: high phytoplankton Fe requirements and (b) scenario 2: low phytoplankton Fe requirements, along Transect 1 in the Barents Sea. Station number is indicated at the top of the plot. Black dots show sample depth at each station. The approximate location of the polar front is denoted by a gray bar. The solid black contour indicates where Fe* equals 0.

To assess whether Fe is limiting phytoplankton productivity in the southwestern Barents Sea, we employed the tracer Fe* (Fe* = [dFe] − (Fe:GLnut) × [GLnut], where (Fe:GLnut) is the average biological uptake ratio of Fe over the growth-limiting macronutrient, nitrate) (Text S2 in Supporting Information S1). Fe* <0 nmol/kg indicates potential Fe-limitation as dFe will be depleted before nitrate. As there is no available information on the nutrient uptake ratios of Arctic phytoplankton, we use the two Fe:N phytoplankton uptake scenarios defined by Rijkenberg et al. (2018), where scenario 1 has high Fe requirements by phytoplankton, and scenario 2 has lower Fe requirements, assuming Arctic phytoplankton have an Fe:N uptake ratio somewhere in between (Text S2 in Supporting Information S1). We found potentially Fe-limiting waters between 20 and 100 m at Stations N01 and N03 under scenario 1 (Figure 9a). This area of potential Fe-limitation coincides with the very low dFe concentrations (Figure 3). Elsewhere in the Atlantic sector, Fe* was close to zero (<0.3) in the upper 150 m under scenario 1 (Stations N02, N04, and N05), and in the upper 100 m of Stations N01–N05 under scenario 2 (Figure 9b). These low Fe* values indicate that, while not at limiting levels, dFe was low at the time of sampling in these areas, which suggests potential Fe-limitation may develop later in the summer bloom period, as dFe is further depleted. Sampling later in the growing season (mid-August to mid-October), Rijkenberg et al. (2018) also found potential Fe-limitation under Fe* scenario 1 along a north–south transect across the Bear Island Trough, intersecting Station N04 from this study.

Nitrate is considered to be the primary limiting nutrient in much of the Arctic Ocean, including the Barents Sea, declining to low concentrations following the spring bloom as strong stratification inhibits nutrient resupply from deep water and lateral nitrate supply from central Arctic waters is low (Krisch et al., 2020; Mills et al., 2018; Taylor et al., 2013; Tuerena et al., 2021). Consistent with this, we observed low concentrations of nitrate (0.01–3.22 μmol/L) across the surface of the Barents Sea (Figure S3 in Supporting Information S1). Thus, productivity in the southwestern Barents Sea is more likely governed by Fe-N co-limitation. A similar nutrient co-limitation regime has been observed in the neighboring Fram Strait, where nitrate is the primary limiting nutrient,

with conditions approaching secondary Fe-limitation (Krisch et al., 2020). This potential Fe-limitation is more akin to the limitation patterns of the high latitude North Atlantic, where several studies have found seasonal Fe-limitation (Achterberg et al., 2018; Birchill et al., 2019; Ryan-Keogh et al., 2013).

The potential for some form of seasonal Fe and N co-limiting regime in the southwestern Barents Sea is influenced by the region's limited access to external Fe and N sources. Isolated from the highly localized external Fe inputs elucidated in this study, the southwestern Barents Sea relies on entrainment during the wintertime deepening of the mixed layer depth (MLD) to replenish dFe in the surface waters (Rigby et al., 2020; Tagliabue et al., 2014). A key control on the vertical supply of dFe to the mixed layer is the strength and depth of the ferricline (depth at which the change in dFe concentration with depth is greatest), relative to the winter MLD (Tagliabue et al., 2014). When the ferricline lies below the winter MLD, Fe inputs are limited, whereas a shallow ferricline enhances resupply. Based on our dFe observations, we calculated the depth of the ferricline relative to the winter MLD along the Atlantic sector of Transect 1 (Stations N01–N06) (Table S4 in Supporting Information S1). In the Barents Sea, the average winter MLD is ∼168 m (Peralta-Ferriz & Woodgate, 2015), while off-shelf in the AW of the Norwegian Sea it typically deepens to 210–250 m (Bagøien et al., 2012). Off the shelf (Stations N01 and N02), the ferricline was considerably deeper than the winter MLD (826 and 350 m, respectively), consistent with patterns typically observed in open-ocean environments (Tagliabue et al., 2014). On the shelf, the ferricline (N03: 125 m; N04 150 m; N05 115 m) was positioned close to the winter MLD. Given the uncertainties in both ferricline and MLD calculations, the ferricline at these stations may even extend below the winter MLD. The depth of the ferricline relative to the winter MLD at these stations likely restricts vertical winter resupply of dFe, driving the near-zero to negative Fe* values observed in this study (Figure 9). In the high latitude North Atlantic Icelandic Basin, Birchill et al. (2019) identified seasonal Fe-limitation, driven by weak vertical resupply and limited lateral transport of shelf-derived Fe to the surface waters. The emergence of similar conditions in our study indicates a shift in the southwestern Barents Sea from a typical Arctic N-limited regime toward an Atlantic-like seasonally Fe or Fe-N co-limited regime. This shift is likely driven by Atlantification of the Barents Sea, where increased inflow of Fe-poor AW, increasing salinity, and surface temperatures result in stronger summer surface stratification (Hordoir et al., 2022) and decreased vertical supply of nutrients (Mousing et al., 2023; Vancoppenolle et al., 2013).

5. Future Implications

Continued Arctic warming is projected to enhance the northward ingress of AW into the Barents Sea (Årthun et al., 2025; Polyakov et al., 2025), with coupled climate model simulations indicating that the region may become ice-free for the entire year toward the end of the century (Årthun et al., 2021). Concurrent with this transition, models predict the largest increases in primary productivity in the northern Barents Sea (Årthun et al., 2025; Bopp et al., 2013; Kwiatkowski et al., 2020; Vancoppenolle et al., 2013), due to greater penetration of light into the upper ocean following sea ice reduction, combined with weakened stratification and deepening of the mixed-layer, that facilitates the upward advection of nutrient-rich AW (Fransner et al., 2023; Noh et al., 2024; Randelhoff et al., 2018). Together, these changes are expected to alleviate limitations in temperature, light availability, and macronutrient supply, to sustain enhanced primary production in the northern Barents Sea (Noh et al., 2024). However, substantial uncertainties remain regarding changes in the biogeochemical cycling of Fe and Mn. An important uncertainty is the loss of dFe and dMn inputs from sea ice. Although our results show that sea ice melt was a minor source of dFe and dMn to the surface waters of the northern Barents Sea at the time of sampling, other studies suggest that sea ice melt can supply Fe and Mn at the initial melt period but subsequently dilutes concentrations of Fe and Mn in the surface ocean (Marsay et al., 2017). However, the loss of sea ice in the northern Barents Sea would remove any inputs of Fe and Mn associated with melt, which could potentially limit future productivity. However, the reduction in Fe and Mn supplied by sea ice may be offset by increased inputs from continental margin sediments, driven by enhanced shelf–water interactions as sea ice cover declines (Tessin et al., 2020). In addition, accelerating glacial melt is expected to increase the supply of nutrients, including Fe and Mn, to the surrounding waters (Meire et al., 2017). However, in Storfjorden, these inputs will be largely confined to the fjord system, where limited exchange restricts transport of Fe and Mn to the wider Barents Sea. As a result, the contribution of these increased inputs to basin-scale primary productivity may be limited. In the southern Barents Sea, increasing surface temperatures will lead to more intense surface stratification, with the MLD decreasing by 17 ± 31 m year-round (Årthun et al., 2025). The shoaling of the MLD will further decrease the vertical supply of nutrients (Mousing et al., 2023; Vancoppenolle et al., 2013), including Fe and Mn. Under these

conditions, Fe or Fe–N co-limitation may become more spatially widespread in the Barents Sea and emerge earlier in the phytoplankton bloom season. Future Atlantification of the Barents Sea may therefore be characterized by a transition to an Atlantic-like nutrient limitation regime, with a widening imbalance between increasing biological demand for Fe and Mn, and a reduction in their supply from both external inputs and vertical fluxes.

6. Conclusions

Using high resolution measurements, this study identified the main external sources of dissolved Fe and Mn in the Barents Sea. Surface enrichment of dFe and dMn adjacent to freshwater inputs indicate that glacial melt constitutes the predominant source of surface water, with sea ice melt as a minor, seasonally influenced source. In the subsurface waters, Fe and Mn maxima are strongly associated with a minima in beam transmission, consistent with inputs from sediment resuspension events to bottom waters. Despite being pronounced, these inputs of dFe and dMn appear spatially constrained, with little lateral or vertical transport away from the source region. Moreover, we found high rates of primary productivity which depleted dFe and dMn in the surface waters of the southwestern Barents Sea, with evidence for seasonal Fe-limitation due to limited vertical resupply of Fe to this highly productive region. These findings do not align with the N-limited regime typical of the Arctic but are more similar to the high latitude North Atlantic, where seasonal Fe-limitation has been observed. This suggests that the southwestern Barents Sea is transitioning to a more Atlantic-like Fe-limited regime as a consequence of Atlantification. Continued Atlantification will advect Fe-poor AW further north-eastward into the Barents Sea, simultaneously reducing sea ice inputs of Fe and Mn and increasing biological demand. This may expand Fe-limitation in the Barents Sea, impacting rates of primary productivity and carbon uptake at a basin-wide scale, and hence the global climate.

Conflict of Interest

The authors declare no conflicts of interest relevant to this study.

Availability Statement

The data presented in this study are archived at the British Oceanographic Data Centre and are publicly available in Lohan et al. (2026), Mahaffey, Norman, et al. (2026), Mahaffey, Fisher, et al. (2026), and Schlitzer (2018).

Acknowledgments
We would like to acknowledge the officers and crew onboard the *RRS Discovery* for their professional and efficient support in facilitating sample and data collection during DY167. ML, CM, and JH were funded by UKRI-NERC Grants (NE/T000570/1 and NE/T001240/1) held at the University of Southampton, the University of Liverpool and the National Oceanography Centre Liverpool. The participation of RS and MM was funded by the NERC project NE/W004933/1 (BIOPOLE). Additional funding for RH comes from the National Environmental Research Council INSPIRE Doctoral Training Partnership (NE/S007210/1).

References

Achterberg, E. P., Steigenberger, S., Marsay, C. M., LeMoigne, F. A. C., Painter, S. C., Baker, A. R., et al. (2018). Iron biogeochemistry in the high latitude North Atlantic Ocean. *Scientific Reports*, *8*(1), 1283. https://doi.org/10.1038/s41598-018-19472-1

Aciego, S. M., Stevenson, E. I., & Arendt, C. A. (2015). Climate versus geological controls on glacial meltwater micronutrient production in southern Greenland. *Earth and Planetary Science Letters*, *424*, 51–58. https://doi.org/10.1016/j.epsl.2015.05.017

Aguilar-Islas, A. M., Rember, R., Nishino, S., Kikuchi, T., & Itoh, M. (2013). Partitioning and lateral transport of iron to the Canada Basin. *Polar Science*, *7*(2), 82–99. https://doi.org/10.1016/j.polar.2012.11.001

Aguilar-Islas, A. M., Rember, R. D., Mordy, C. W., & Wu, J. (2008). Sea ice-derived dissolved iron and its potential influence on the spring algal bloom in the Bering Sea. *Geophysical Research Letters*, *35*(24). https://doi.org/10.1029/2008GL035736

Annett, A. L., Skiba, M., Henley, S. F., Venables, H. J., Meredith, M. P., Statham, P. J., & Ganeshram, R. S. (2015). Comparative roles of upwelling and glacial iron sources in Ryder Bay, coastal western Antarctic Peninsula. *Marine Chemistry*, *176*, 21–33. https://doi.org/10.1016/j.marchem.2015.06.017

Arrigo, K. R., van Dijken, G., & Pabi, S. (2008). Impact of a shrinking Arctic ice cover on marine primary production. *Geophysical Research Letters*, *35*(19), L11501. https://doi.org/10.1029/2008GL035028

Arrigo, K. R., & van Dijken, G. L. (2015). Continued increases in Arctic Ocean primary production. *Progress in Oceanography*, *136*, 60–70. https://doi.org/10.1016/j.pocean.2015.05.002

Årthun, M., Dinh, K. V., Dörr, J., Dupont, N., Fransner, F., Nilsen, I., et al. (2025). The future Barents Sea—A synthesis of physical, biogeochemical, and ecological changes toward 2050 and 2100. *Elementa: Science of the Anthropocene*, *13*(1), 00046. https://doi.org/10.1525/elementa.2024.00046

Årthun, M., Eldevik, T., Smedsrud, L. H., Skagseth, Ø., & Ingvaldsen, R. B. (2012). Quantifying the influence of Atlantic heat on Barents Sea ice variability and retreat. https://doi.org/10.1175/JCLI-D-11-00466.1

Årthun, M., Onarheim, I. H., Dörr, J., & Eldevik, T. (2021). The seasonal and regional transition to an ice-free Arctic. *Geophysical Research Letters*, *48*(1), e2020GL090825. https://doi.org/10.1029/2020GL090825

Bagøien, E., Melle, W., & Kaartvedt, S. (2012). Seasonal development of mixed layer depths, nutrients, chlorophyll and *Calanus finmarchicus* in the Norwegian Sea—A basin-scale habitat comparison. *Progress in Oceanography*, *103*, 58–79. https://doi.org/10.1016/j.pocean.2012.04.014

Barton, B. I., Lenn, Y.-D., & Lique, C. (2018). Observed Atlantification of the Barents Sea causes the polar front to limit the expansion of Winter Sea ice. *Journal of Physical Oceanography*, *48*(8), 1849–1866. https://doi.org/10.1175/JPO-D-18-0003.1

Barton, B. I., Lique, C., & Lenn, Y.-D. (2020). Water mass properties derived from satellite observations in the Barents Sea. *Journal of Geophysical Research: Oceans*, *125*(8), e2019JC015449. https://doi.org/10.1029/2019JC015449

Bhatia, M. P., Kujawinski, E. B., Das, S. B., Breier, C. F., Henderson, P. B., & Charette, M. A. (2013). Greenland meltwater as a significant and potentially bioavailable source of iron to the ocean. *Nature Geoscience*, *6*(4), 274–278. https://doi.org/10.1038/ngeo1746

Birchill, A. J., Hartner, N. T., Kunde, K., Siemering, B., Daniels, C., González-Santana, D., et al. (2019). The eastern extent of seasonal iron limitation in the high latitude North Atlantic Ocean. *Scientific Reports*, *9*(1), 1435. https://doi.org/10.1038/s41598-018-37436-3

Błaszczyk, M., Jania, J. A., & Hagen, J. O. (2009). Tidewater glaciers of Svalbard: Recent changes and estimates of calving fluxes. *Polish Polar Research*, *30*(2), 85–142.

Bopp, L., Resplandy, L., Orr, J. C., Doney, S. C., Dunne, J. P., Gehlen, M., et al. (2013). Multiple stressors of ocean ecosystems in the 21st century: Projections with CMIP5 models. *Biogeosciences*, *10*(10), 6225–6245. https://doi.org/10.5194/bg-10-6225-2013

Boyd, P. W., & Ellwood, M. J. (2010). The biogeochemical cycle of iron in the ocean. *Nature Geoscience*, *3*(10), 675–682. https://doi.org/10.1038/ngeo964

Browning, T. J., Achterberg, E. P., Engel, A., & Mawji, E. (2021). Manganese co-limitation of phytoplankton growth and major nutrient drawdown in the Southern Ocean. *Nature Communications*, *12*(1), 884. https://doi.org/10.1038/s41467-021-21122-6

Bruland, K. W., Donat, J. R., & Hutchins, D. A. (1991). Interactive influences of bioactive trace metals on biological production in oceanic waters. *Limnology & Oceanography*, *36*(8), 1555–1577. https://doi.org/10.4319/lo.1991.36.8.1555

Bruland, K. W., & Lohan, M. C. (2003). 6.02—Controls of trace metals in seawater. In H. D. Holland & K. K. Turekian (Eds.), *Treatise on geochemistry* (pp. 23–47). Pergamon. https://doi.org/10.1016/B0-08-043751-6/06105-3

Bruland, K. W., Orians, K. J., & Cowen, J. P. (1994). Reactive trace metals in the stratified central North Pacific. *Geochimica et Cosmochimica Acta*, *58*(15), 3171–3182. https://doi.org/10.1016/0016-7037(94)90044-2

Carmack, E., & Wassmann, P. (2006). Food webs and physical–biological coupling on pan-arctic shelves: Unifying concepts and comprehensive perspectives. *Progress in Oceanography*, *71*(2), 446–477. https://doi.org/10.1016/j.pocean.2006.10.004

Castro de la Guardia, L., Hernández Fariñas, T., Marchese, C., Amargant-Arumí, M., Myers, P. G., Bélanger, S., et al. (2023). Assessing net primary production in the northwestern Barents Sea using in situ, remote sensing and modelling approaches. *Progress in Oceanography*, *219*, 103160. https://doi.org/10.1016/j.pocean.2023.103160

Colombo, M., Jackson, S. L., Cullen, J. T., & Orians, K. J. (2020). Dissolved iron and manganese in the Canadian Arctic Ocean: On the biogeochemical processes controlling their distributions. *Geochimica et Cosmochimica Acta*, *277*, 150–174. https://doi.org/10.1016/j.gca.2020.03.012

Colombo, M., Li, J., Rogalla, B., Allen, S. E., & Maldonado, M. T. (2022). Particulate trace element distributions along the Canadian Arctic GEOTRACES section: Shelf-water interactions, advective transport and contrasting biological production. *Geochimica et Cosmochimica Acta*, *323*, 183–201. https://doi.org/10.1016/j.gca.2022.02.013

Colombo, M., Rogalla, B., Li, J., Allen, S. E., Orians, K. J., & Maldonado, M. T. (2021). Canadian arctic Archipelago Shelf-Ocean interactions: A major iron source to Pacific derived waters transiting to the Atlantic. *Global Biogeochemical Cycles*, *35*(10), e2021GB007058. https://doi.org/10.1029/2021GB007058

Comiso, J. C. (2012). Large decadal decline of the Arctic multiyear ice cover. https://doi.org/10.1175/JCLI-D-11-00113.1

Dalpadado, P., Arrigo, K. R., Hjøllo, S. S., Rey, F., Ingvaldsen, R. B., Sperfeld, E., et al. (2014). Productivity in the Barents Sea - Response to recent climate variability. *PLoS One*, *9*(5), e95273. https://doi.org/10.1371/journal.pone.0095273

de Baar, H. J. W., & de Jong, J. T. M. (2001). Distributions, sources and sinks of iron in seawater. In D. Turner & K. A. Hunter (Eds.), *Biogeochemistry of iron in seawater* (pp. 123–253). Wiley.

Elderfield, H., & Schultz, A. (1996). Mid-Ocean Ridge hydrothermal fluxes and the chemical composition of the Ocean. *Annual Review of Earth and Planetary Sciences*, *24*(24), 191–224. https://doi.org/10.1146/annurev.earth.24.1.191

Faust, J. C., Stevenson, M. A., Abbott, G. D., Knies, J., Tessin, A., Mannion, I., et al. (2020). Does Arctic warming reduce preservation of organic matter in Barents Sea sediments? *Philosophical Transactions of the Royal Society A: Mathematical, Physical and Engineering Sciences*, *378*(2181), 20190364. https://doi.org/10.1098/rsta.2019.0364

Fer, I., & Drinkwater, K. (2014). Mixing in the Barents Sea polar front near hopen in spring. *Journal of Marine Systems*, *130*, 206–218. https://doi.org/10.1016/j.jmarsys.2012.01.005

Field, C. B., Behrenfeld, M. J., Randerson, J. T., & Falkowski, P. (1998). Primary production of the biosphere: Integrating terrestrial and Oceanic components. *Science*, *281*(5374), 237–240. https://doi.org/10.1126/science.281.5374.237

Fransner, F., Olsen, A., Årthun, M., Counillon, F., Tjiputra, J., Samuelsen, A., & Keenlyside, N. (2023). Phytoplankton abundance in the Barents Sea is predictable up to five years in advance. *Communications Earth & Environment*, *4*(1), 141. https://doi.org/10.1038/s43247-023-00791-9

Froelich, P. N., Klinkhammer, G. P., Bender, M. L., Luedtke, N. A., Heath, G. R., Cullen, D., et al. (1979). Early oxidation of organic matter in pelagic sediments of the eastern equatorial Atlantic: Suboxic diagenesis. *Geochimica et Cosmochimica Acta*, *43*(7), 1075–1090. https://doi.org/10.1016/0016-7037(79)90095-4

Gerringa, L. J. A., Rijkenberg, M. J. A., Slagter, H. A., Laan, P., Paffrath, R., Bauch, D., et al. (2021). Dissolved Cd, Co, Cu, Fe, Mn, Ni, and Zn in the Arctic Ocean. *Journal of Geophysical Research: Oceans*, *126*(9), e2021JC017323. https://doi.org/10.1029/2021JC017323

Grotti, M., Soggia, F., Ianni, C., & Frache, R. (2005). Trace metals distributions in coastal sea ice of Terra Nova Bay, Ross Sea, Antarctica. *Antarctic Science*, *17*(2), 289–300. https://doi.org/10.1017/S0954102005002695

Gruber, N., & Sarmiento, J. L. (1997). Global patterns of marine nitrogen fixation and denitrification. *Global Biogeochemical Cycles*, *11*(2), 235–266. https://doi.org/10.1029/97GB00077

Guieu, C., Huang, W. W., Martin, J.-M., & Yong, Y. Y. (1996). Outflow of trace metals into the Laptev Sea by the Lena River. *Marine Chemistry*, *53*(3), 255–267. https://doi.org/10.1016/0304-4203(95)00093-3

Hatta, M., Measures, C. I., Wu, J., Roshan, S., Fitzsimmons, J. N., Sedwick, P., & Morton, P. (2015). An overview of dissolved Fe and Mn distributions during the 2010–2011 U.S. GEOTRACES north Atlantic cruises: Geotraces GA03. *Deep Sea Research Part II: Topical Studies in Oceanography*, *116*, 117–129. https://doi.org/10.1016/j.dsr2.2014.07.005

Hawco, N. J., Tagliabue, A., & Twining, B. S. (2022). Manganese limitation of Phytoplankton physiology and productivity in the Southern Ocean. *Global Biogeochemical Cycles*, *36*(11), e2022GB007382. https://doi.org/10.1029/2022GB007382

Hawkings, J. R., Skidmore, M. L., Wadham, J. L., Priscu, J. C., Morton, P. L., Hatton, J. E., et al. (2020). Enhanced trace element mobilization by Earth's ice sheets. *Proceedings of the National Academy of Sciences*, *117*(50), 31648–31659. https://doi.org/10.1073/pnas.2014378117

Hopwood, M. J., Cantoni, C., Clarke, J. S., Cozzi, S., & Achterberg, E. P. (2017). The heterogeneous nature of Fe delivery from melting icebergs. *Geochemical Perspectives Letters*, *3*, 200–209. https://doi.org/10.7185/geochemlet.1723

Hopwood, M. J., Connelly, D. P., Arendt, K. E., Juul-Pedersen, T., Stinchcombe, M. C., Meire, L., et al. (2016). Seasonal changes in Fe along a glaciated Greenlandic fjord. *Frontiers in Earth Science*, *4*, 15. https://doi.org/10.3389/feart.2016.00015

Hordoir, R., Skagseth, Ø., Ingvaldsen, R. B., Sandø, A. B., Löptien, U., Dietze, H., et al. (2022). Changes in arctic stratification and mixed layer depth cycle: A modeling analysis. *Journal of Geophysical Research: Oceans*, *127*(1), e2021JC017270. https://doi.org/10.1029/2021JC017270

Ilyas, M., Hopkins, J., Mahaffey, C., & Norman, L. (2026). Classification of Barents Sea water masses from cruise DY167 (RRS discovery) in July-August 2023 using Optimum Multiparameter (OMP) analysis [Dataset]. *Zenodo*. https://doi.org/10.5281/zenodo.18619607

Jakobsson, M. (2002). Hypsometry and volume of the Arctic Ocean and its constituent seas. *Geochemistry, Geophysics, Geosystems*, *3*(5), 1–18. https://doi.org/10.1029/2001GC000302

Jeandel, C., & Oelkers, E. H. (2015). The influence of terrigenous particulate material dissolution on ocean chemistry and global element cycles. *Chemical Geology*, *395*, 50–66. https://doi.org/10.1016/j.chemgeo.2014.12.001

Jensen, L. T., Morton, P., Twining, B. S., Heller, M. I., Hatta, M., Measures, C. I., et al. (2020). A comparison of marine Fe and Mn cycling: U.S. GEOTRACES GN01 Western Arctic case study. *Geochimica et Cosmochimica Acta*, *288*, 138–160. https://doi.org/10.1016/j.gca.2020.08.006

Jickells, T. (1995). Atmospheric inputs of metals and nutrients to the oceans: Their magnitude and effects. *Marine Chemistry*, *48*(3), 199–214. https://doi.org/10.1016/0304-4203(95)92784-P

Johnson, K. S., Chavez, F. P., & Friederich, G. E. (1999). Continental-shelf sediment as a primary source of iron for coastal phytoplankton. *Nature*, *398*(6729), 697–700. https://doi.org/10.1038/19511

Jones, M. T., Gislason, S. R., Burton, K. W., Pearce, C. R., Mavromatis, V., Pogge von Strandmann, P. A. E., & Oelkers, E. H. (2014). Quantifying the impact of riverine particulate dissolution in seawater on ocean chemistry. *Earth and Planetary Science Letters*, *395*, 91–100. https://doi.org/10.1016/j.epsl.2014.03.039

Jones, M. T., Pearce, C. R., Jeandel, C., Gislason, S. R., Eiriksdottir, E. S., Mavromatis, V., & Oelkers, E. H. (2012). Riverine particulate material dissolution as a significant flux of strontium to the oceans. *Earth and Planetary Science Letters*, *355–356*, 51–59. https://doi.org/10.1016/j.epsl.2012.08.040

Jones, R. L., Hawkings, J. R., Meredith, M. P., Lohan, M. C., Moore, O. W., Sherrell, R. M., et al. (2025). Antarctic glaciers export carbon-stabilised iron(II)-rich particles to the surface Southern Ocean. *Nature Communications*, *16*(1), 5015. https://doi.org/10.1038/s41467-025-59981-y

Kanna, N., Sugiyama, S., Fukamachi, Y., Nomura, D., & Nishioka, J. (2020). Iron supply by subglacial discharge into a fjord near the front of a marine-terminating Glacier in Northwestern Greenland. *Global Biogeochemical Cycles*, *34*(10), e2020GB006567. https://doi.org/10.1029/2020GB006567

Kanna, N., Sugiyama, S., Ohashi, Y., Sakakibara, D., Fukamachi, Y., & Nomura, D. (2018). Upwelling of macronutrients and dissolved inorganic carbon by a subglacial freshwater driven plume in bowdoin fjord, Northwestern Greenland. *Journal of Geophysical Research: Biogeosciences*, *123*(5), 1666–1682. https://doi.org/10.1029/2017JG004248

Kanna, N., Tateyama, K., Waseda, T., Timofeeva, A., Papadimitraki, M., Whitmore, L., et al. (2025). Spatial distributions of iron and manganese in surface waters of the Arctic's Laptev and East Siberian seas. *Biogeosciences*, *22*(4), 1057–1076. https://doi.org/10.5194/bg-22-1057-2025

Kanna, N., Toyota, T., & Nishioka, J. (2014). Iron and macro-nutrient concentrations in sea ice and their impact on the nutritional status of surface waters in the southern Okhotsk Sea. *Progress in Oceanography*, *126*, 44–57. https://doi.org/10.1016/j.pocean.2014.04.012

Klunder, M. B., Bauch, D., Laan, P., de Baar, H. J. W., van Heuven, S., & Ober, S. (2012). Dissolved iron in the Arctic shelf seas and surface waters of the central Arctic Ocean: Impact of Arctic river water and ice-melt. *Journal of Geophysical Research*, *117*(C1). https://doi.org/10.1029/2011JC007133

Klunder, M. B., Laan, P., Middag, R., de Baar, H. J. W., & Bakker, K. (2012). Dissolved iron in the Arctic Ocean: Important role of hydrothermal sources, shelf input and scavenging removal. *Journal of Geophysical Research*, *117*(C4). https://doi.org/10.1029/2011JC007135

Kondo, Y., Obata, H., Hioki, N., Ooki, A., Nishino, S., Kikuchi, T., & Kuma, K. (2016). Transport of trace metals (Mn, Fe, Ni, Zn and Cd) in the western Arctic Ocean (Chukchi Sea and Canada Basin) in late summer 2012. *Deep Sea Research Part I: Oceanographic Research Papers*, *116*, 236–252. https://doi.org/10.1016/j.dsr.2016.08.010

Krause, J., Hopwood, M. J., Höfer, J., Krisch, S., Achterberg, E. P., Alarcón, E., et al. (2021). Trace element (Fe, Co, Ni and Cu) dynamics across the salinity gradient in Arctic and antarctic Glacier fjords. *Frontiers in Earth Science*, *9*, 725279. https://doi.org/10.3389/feart.2021.725279

Krisch, S., Browning, T. J., Graeve, M., Ludwichowski, K.-U., Lodeiro, P., Hopwood, M. J., et al. (2020). The influence of Arctic Fe and Atlantic fixed N on summertime primary production in Fram Strait, North Greenland Sea. *Scientific Reports*, *10*(1), 15230. https://doi.org/10.1038/s41598-020-72100-9

Kunde, K., Wyatt, N. J., González-Santana, D., Tagliabue, A., Mahaffey, C., & Lohan, M. C. (2019). Iron distribution in the subtropical north Atlantic: The pivotal role of colloidal iron. *Global Biogeochemical Cycles*, *33*(12), 1532–1547. https://doi.org/10.1029/2019GB006326

Kwiatkowski, L., Torres, O., Bopp, L., Aumont, O., Chamberlain, M., Christian, J. R., et al. (2020). Twenty-first century ocean warming, acidification, deoxygenation, and upper-ocean nutrient and primary production decline from CMIP6 model projections. *Biogeosciences*, *17*(13), 3439–3470. https://doi.org/10.5194/bg-17-3439-2020

Landing, W. M., & Bruland, K. W. (1987). The contrasting biogeochemistry of iron and manganese in the Pacific Ocean. *Geochimica et Cosmochimica Acta*, *51*(1), 29–43. https://doi.org/10.1016/0016-7037(87)90004-4

Lannuzel, D., Schoemann, V., de Jong, J., Chou, L., Delille, B., Becquevort, S., & Tison, J.-L. (2008). Iron study during a time series in the western Weddell pack ice. *Marine Chemistry*, *108*(1), 85–95. https://doi.org/10.1016/j.marchem.2007.10.006

Lannuzel, D., Schoemann, V., de Jong, J., Tison, J.-L., & Chou, L. (2007). Distribution and biogeochemical behaviour of iron in the East Antarctic sea ice. *Marine Chemistry*, *106*(1), 18–32. https://doi.org/10.1016/j.marchem.2006.06.010

Lee, Y. J., Matrai, P. A., Friedrichs, M. A. M., Saba, V. S., Antoine, D., Ardyna, M., et al. (2015). An assessment of phytoplankton primary productivity in the Arctic Ocean from satellite ocean color/in situ chlorophyll-a based models. *Journal of Geophysical Research: Oceans*, *120*(9), 6508–6541. https://doi.org/10.1002/2015JC011018

Lewis, K. M., van Dijken, G. L., & Arrigo, K. R. (2020). Changes in phytoplankton concentration now drive increased Arctic Ocean primary production. *Science*, *369*(6500), 198–202. https://doi.org/10.1126/science.aay8380

Lind, S., Ingvaldsen, R. B., & Furevik, T. (2016). Arctic layer salinity controls heat loss from deep Atlantic layer in seasonally ice-covered areas of the Barents Sea. *Geophysical Research Letters*, *43*(10), 5233–5242. https://doi.org/10.1002/2016GL068421

Lind, S., Ingvaldsen, R. B., & Furevik, T. (2018). Arctic warming hotspot in the northern Barents Sea linked to declining sea-ice import. *Nature Climate Change*, *8*(7), 634–639. https://doi.org/10.1038/s41558-018-0205-y

Lippiatt, S. M., Lohan, M. C., & Bruland, K. W. (2010). The distribution of reactive iron in northern Gulf of Alaska coastal waters. *Marine Chemistry*, *121*(1), 187–199. https://doi.org/10.1016/j.marchem.2010.04.007

Loeng, H. (1991). Features of the physical oceanographic conditions of the Barents Sea. *Polar Research*, *10*(1), 5–18. https://doi.org/10.3402/polar.v10i1.6723

Lohan, M. C., Aguilar-Islas, A. M., & Bruland, K. W. (2006). Direct determination of iron in acidified (pH 1.7) seawater samples by flow injection analysis with catalytic spectrophotometric detection: Application and intercomparison. *Limnology and Oceanography: Methods*, *4*(6), 164–171. https://doi.org/10.4319/lom.2006.4.164

Lohan, M. C., Hawley, R., Flanagan, O., Mahaffey, C., Norman, L., Hopkins, J., et al. (2026). Titanium CTD water column samples (macronutrients, chlorophyll-a, trace elements) and upcast sensor measurements (temperature, salinity, oxygen, optical backscatter, beam transmittance and attenuation, PAR, fluorescence) from the Norwegian and Barents Sea on cruise DY167 (GApr19), July-August 2023 [Dataset]. *NERC EDS British Oceanographic Data Centre NOC*. https://doi.org/10.5285/48c1d94c-1647-8717-e063-7086abc0f520

Mahaffey, C., Fisher, B. J., Wrightson, L., Hopkins, J., Arrowsmith, C., Sanders, R. N. C., et al. (2026). Stainless Steel CTD water column samples (macronutrients, chlorophyll-a, particulate carbon, C-fixation, d18O) and upcast sensor measurements (temperature, salinity, oxygen, optical backscatter, beam transmittance and attenuation, PAR, fluorescence) from cruise DY167 (GApr19), July-August 2023 [Dataset]. *NERC EDS British Oceanographic Data Centre NOC*. https://doi.org/10.5285/48e39c93-2405-99f3-e063-7086abc003fa

Mahaffey, C., Norman, L., Fisher, B. J., Wrightson, L., Lohan, M. C., Hawley, R., et al. (2026). Underway biogeochemical samples data (macronutrients, chlorophyll-a, dissolved trace elements, particulate carbon, carbon fixation, d18O) and water mass fractions from a Towfish at 3 m in the Norwegian and Barents Sea on cruise DY167 (GApr19), July-August 2023 [Dataset]. *NERC EDS British Oceanographic Data Centre NOC*. https://doi.org/10.5285/48d50e6a-e137-e1e3-e063-7086abc09a72

Mankoff, K. D., Straneo, F., Cenedese, C., Das, S. B., Richards, C. G., & Singh, H. (2016). Structure and dynamics of a subglacial discharge plume in a Greenlandic fjord. *Journal of Geophysical Research: Oceans*, *121*(12), 8670–8688. https://doi.org/10.1002/2016JC011764

Marsay, C. M., Barrett, P. M., McGillicuddy, D. J., Jr., & Sedwick, P. N. (2017). Distributions, sources, and transformations of dissolved and particulate iron on the Ross Sea continental shelf during summer. *Journal of Geophysical Research: Oceans*, *122*(8), 6371–6393. https://doi.org/10.1002/2017JC013068

Martin, J. H. (1990). Glacial-interglacial CO2 change: The Iron Hypothesis. *Paleoceanography*, *5*(1), 1–13. https://doi.org/10.1029/PA005i001p00001

Measures, C. I. (1999). The role of entrained sediments in sea ice in the distribution of aluminium and iron in the surface waters of the Arctic Ocean. *Marine Chemistry*, *68*(1), 59–70. https://doi.org/10.1016/S0304-4203(99)00065-1

Meire, L., Mortensen, J., Meire, P., Juul-Pedersen, T., Sejr, M. K., Rysgaard, S., et al. (2017). Marine-terminating glaciers sustain high productivity in Greenland fjords. *Global Change Biology*, *23*(12), 5344–5357. https://doi.org/10.1111/gcb.13801

Michael, S. M., Crusius, J., Schroth, A. W., Campbell, R., & Resing, J. A. (2023). Glacial meltwater and sediment resuspension can be important sources of dissolved and total dissolvable aluminum and manganese to coastal ocean surface waters. *Limnology & Oceanography*, *68*(6), 1201–1215. https://doi.org/10.1002/lno.12339

Middag, R., De Baar, H. J. W., Laan, P., & Klunder, M. B. (2011). Fluvial and hydrothermal input of manganese into the Arctic Ocean. *Geochimica et Cosmochimica Acta*, *75*(9), 2393–2408. https://doi.org/10.1016/j.gca.2011.02.011

Millero, F. J., Sotolongo, S., & Izaguirre, M. (1987). The oxidation kinetics of Fe(II) in seawater. *Geochimica et Cosmochimica Acta*, *51*(4), 793–801. https://doi.org/10.1016/0016-7037(87)90093-7

Mills, M. M., Brown, Z. W., Laney, S. R., Ortega-Retuerta, E., Lowry, K. E., van Dijken, G. L., & Arrigo, K. R. (2018). Nitrogen limitation of the summer phytoplankton and heterotrophic prokaryote communities in the Chukchi Sea. *Frontiers in Marine Science*, *5*, 362. https://doi.org/10.3389/fmars.2018.00362

Milne, A., Landing, W., Bizimis, M., & Morton, P. (2010). Determination of Mn, Fe, Co, Ni, Cu, Zn, Cd and Pb in seawater using high resolution magnetic sector inductively coupled mass spectrometry (HR-ICP-MS). *Analytica Chimica Acta*, *665*(2), 200–207. https://doi.org/10.1016/j.aca.2010.03.027

Moore, C. M., Mills, M. M., Arrigo, K. R., Berman-Frank, I., Bopp, L., Boyd, P. W., et al. (2013). Processes and patterns of oceanic nutrient limitation. *Nature Geoscience*, *6*(9), 701–710. https://doi.org/10.1038/ngeo1765

Moore, J. K., & Braucher, O. (2008). Sedimentary and mineral dust sources of dissolved iron to the world ocean. *Biogeosciences*, *5*(3), 631–656. https://doi.org/10.5194/bg-5-631-2008

Moore, J. K., Doney, S. C., Glover, D. M., & Fung, I. Y. (2001). Iron cycling and nutrient-limitation patterns in surface waters of the World Ocean. *Deep Sea Research Part II: Topical Studies in Oceanography*, *49*(1), 463–507. https://doi.org/10.1016/S0967-0645(01)00109-6

Morel, F. M. M., & Price, N. M. (2003). The biogeochemical cycles of trace metals in the Oceans. *Science*, *300*(5621), 944–947. https://doi.org/10.1126/science.1083545

Motyka, R. J., Dryer, W. P., Amundson, J., Truffer, M., & Fahnestock, M. (2013). Rapid submarine melting driven by subglacial discharge, LeConte Glacier, Alaska. *Geophysical Research Letters*, *40*(19), 5153–5158. https://doi.org/10.1002/grl.51011

Mousing, E. A., Ellingen, I., Hjøllo, S. S., Husson, B., Skogen, M. D., & Wallhead, P. (2023). Why do regional biogeochemical models produce contrasting future projections of primary production in the Barents Sea? *Journal of Sea Research*, *192*, 102366. https://doi.org/10.1016/j.seares.2023.102366

Noh, K.-M., Oh, J.-H., Lim, H.-G., Song, H., & Kug, J.-S. (2024). Role of atlantification in enhanced primary productivity in the Barents Sea. *Earth's Future*, *12*(1), e2023EF003709. https://doi.org/10.1029/2023EF003709

Oziel, L., Sirven, J., & Gascard, J.-C. (2016). The Barents Sea frontal zones and water masses variability (1980–2011). *Ocean Science*, *12*(1), 169–184. https://doi.org/10.5194/os-12-169-2016

Pearce, C. R., Jones, M. T., Oelkers, E. H., Pradoux, C., & Jeandel, C. (2013). The effect of particulate dissolution on the neodymium (Nd) isotope and Rare Earth Element (REE) composition of seawater. *Earth and Planetary Science Letters*, *369–370*, 138–147. https://doi.org/10.1016/j.epsl.2013.03.023

Peralta-Ferriz, C., & Woodgate, R. A. (2015). Seasonal and interannual variability of pan-arctic surface mixed layer properties from 1979 to 2012 from hydrographic data, and the dominance of stratification for multiyear mixed layer depth shoaling. *Progress in Oceanography*, *134*, 19–53. https://doi.org/10.1016/j.pocean.2014.12.005

Polyakov, I. V., Pnyushkov, A. V., Alkire, M. B., Ashik, I. M., Baumann, T. M., Carmack, E. C., et al. (2017). Greater role for Atlantic inflows on sea-ice loss in the Eurasian Basin of the Arctic Ocean. *Science*, *356*(6335), 285–291. https://doi.org/10.1126/science.aai8204

Polyakov, I. V., Pnyushkov, A. V., Charette, M., Cho, K.-H., Jung, J., Kipp, L., et al. (2025). Atlantification advances into the Amerasian Basin of the Arctic Ocean. *Science Advances*, *11*(8), eadq7580. https://doi.org/10.1126/sciadv.adq7580

Raiswell, R., Hawkings, J. R., Benning, L. G., Baker, A. R., Death, R., Albani, S., et al. (2016). Potentially bioavailable iron delivery by iceberg-hosted sediments and atmospheric dust to the polar oceans. *Biogeosciences*, *13*(13), 3887–3900. https://doi.org/10.5194/bg-13-3887-2016

Raiswell, R., Tranter, M., Benning, L. G., Siegert, M., De'ath, R., Huybrechts, P., & Payne, T. (2006). Contributions from glacially derived sediment to the global iron (oxyhydr)oxide cycle: Implications for iron delivery to the oceans. *Geochimica et Cosmochimica Acta*, *70*(11), 2765–2780. https://doi.org/10.1016/j.gca.2005.12.027

Randelhoff, A., Reigstad, M., Chierici, M., Sundfjord, A., Ivanov, V., Cape, M., et al. (2018). Seasonality of the physical and biogeochemical hydrography in the inflow to the Arctic Ocean through fram Strait. *Frontiers in Marine Science*, *5*, 224. https://doi.org/10.3389/fmars.2018.00224

Rantanen, M., Karpechko, A. Y., Lipponen, A., Nordling, K., Hyvärinen, O., Ruosteenoja, K., et al. (2022). The Arctic has warmed nearly four times faster than the globe since 1979. *Communications Earth & Environment*, *3*(1), 168. https://doi.org/10.1038/s43247-022-00498-3

Rapp, I., Schlosser, C., Rusiecka, D., Gledhill, M., & Achterberg, E. P. (2017). Automated preconcentration of Fe, Zn, Cu, Ni, Cd, Pb, Co, and Mn in seawater with analysis using high-resolution sector field inductively-coupled plasma mass spectrometry. *Analytica Chimica Acta*, *976*, 1–13. https://doi.org/10.1016/j.aca.2017.05.008

Raven, J. A. (1988). The iron and molybdenum use efficiencies of plant growth with different energy, carbon and nitrogen sources. *New Phytologist*, *109*(3), 279–287. https://doi.org/10.1111/j.1469-8137.1988.tb04196.x

Raven, J. A., Evans, M. C. W., & Korb, R. E. (1999). The role of trace metals in photosynthetic electron transport in O2-evolving organisms. *Photosynthesis Research*, *60*(2), 111–150. https://doi.org/10.1023/A:1006282714942

Reigstad, M., Carroll, J., Slagstad, D., Ellingsen, I., & Wassmann, P. (2011). Intra-regional comparison of productivity, carbon flux and ecosystem composition within the northern Barents Sea. *Progress in Oceanography*, *90*(1), 33–46. https://doi.org/10.1016/j.pocean.2011.02.005

Rigby, S. J., Williams, R. G., Achterberg, E. P., & Tagliabue, A. (2020). Resource availability and entrainment are driven by offsets between nutriclines and Winter mixed-layer depth. *Global Biogeochemical Cycles*, *34*(7), e2019GB006497. https://doi.org/10.1029/2019GB006497

Rijkenberg, M. J. A., Slagter, H. A., Rutgers van der Loeff, M., van Ooijen, J., & Gerringa, L. J. A. (2018). Dissolved Fe in the deep and upper Arctic Ocean with a focus on Fe limitation in the nansen Basin. *Frontiers in Marine Science*, *5*, 88. https://doi.org/10.3389/fmars.2018.00088

Ryan-Keogh, T. J., Macey, A. I., Nielsdóttir, M. C., Lucas, M. I., Steigenberger, S. S., Stinchcombe, M. C., et al. (2013). Spatial and temporal development of phytoplankton iron stress in relation to bloom dynamics in the high-latitude North Atlantic Ocean. *Limnology & Oceanography*, *58*(2), 533–545. https://doi.org/10.4319/lo.2013.58.2.0533

Sakshaug, E. (1997). Biomass and productivity distributions and their variability in the Barents Sea. *ICES Journal of Marine Science*, *54*(3), 341–350. https://doi.org/10.1006/jmsc.1996.0170

Sakshaug, E., & Slagstad, D. (1991). Light and productivity of phytoplankton in polar marine ecosystems: A physiological view. *Polar Research*, *10*(1), 69–86. https://doi.org/10.3402/polar.v10i1.6729

Sarthou, G., Bucciarelli, E., Chever, F., Hansard, S. P., González-Dávila, M., Santana-Casiano, J. M., et al. (2011). Labile Fe(II) concentrations in the Atlantic sector of the Southern Ocean along a transect from the subtropical domain to the Weddell Sea Gyre. *Biogeosciences*, *8*(9), 2461–2479. https://doi.org/10.5194/bg-8-2461-2011

Schlitzer, R. (2018). Ocean Data View. Retrieved from https://odv.awi.de

Schroth, A. W., Crusius, J., Hoyer, I., & Campbell, R. (2014). Estuarine removal of glacial iron and implications for iron fluxes to the ocean. *Geophysical Research Letters*, *41*(11), 3951–3958. https://doi.org/10.1002/2014GL060199

Sedwick, P. N., DiTullio, G. R., & Mackey, D. J. (2000). Iron and manganese in the Ross Sea, Antarctica: Seasonal iron limitation in Antarctic shelf waters. *Journal of Geophysical Research*, *105*(C5), 11321–11336. https://doi.org/10.1029/2000JC000256

Shen, Z., Zhang, R., Ren, J., Marsay, C., Zhu, Z., Wu, Y., et al. (2024). Distribution of dissolved aluminum and dissolved iron in Kongsfjorden: A glacial fjord in the Arctic. *Marine Chemistry*, *263–264*, 104399. https://doi.org/10.1016/j.marchem.2024.104399

Skagseth, Ø. (2008). Recirculation of Atlantic water in the western Barents Sea. *Geophysical Research Letters*, *35*(11). https://doi.org/10.1029/2008GL033785

Smedsrud, L. H., Esau, I., Ingvaldsen, R. B., Eldevik, T., Haugan, P. M., Li, C., et al. (2013). The role of the Barents Sea in the Arctic climate system. *Reviews of Geophysics*, *51*(3), 415–449. https://doi.org/10.1002/rog.20017

Sunda, W. G. (2012). Feedback interactions between trace metal nutrients and phytoplankton in the Ocean. *Frontiers in Microbiology*, *3*. https://doi.org/10.3389/fmicb.2012.00204

Sunda, W. G., & Huntsman, S. A. (1988). Effect of sunlight on redox cycles of manganese in the southwestern Sargasso Sea. *Deep-Sea Research, Part A: Oceanographic Research Papers*, *35*(8), 1297–1317. https://doi.org/10.1016/0198-0149(88)90084-2

Sunda, W. G., & Huntsman, S. A. (1994). Photoreduction of manganese oxides in seawater. *Marine Chemistry*, *46*(1), 133–152. https://doi.org/10.1016/0304-4203(94)90051-5

Tagliabue, A., Aumont, O., & Bopp, L. (2014). The impact of different external sources of iron on the global carbon cycle. *Geophysical Research Letters*, *41*(3), 920–926. https://doi.org/10.1002/2013GL059059

Tagliabue, A., Bowie, A. R., Boyd, P. W., Buck, K. N., Johnson, K. S., & Saito, M. A. (2017). The integral role of iron in ocean biogeochemistry. *Nature*, *543*(7643), 51–59. https://doi.org/10.1038/nature21058

Taylor, R. L., Semeniuk, D. M., Payne, C. D., Zhou, J., Tremblay, J.-É., Cullen, J. T., & Maldonado, M. T. (2013). Colimitation by light, nitrate, and iron in the Beaufort Sea in late summer. *Journal of Geophysical Research: Oceans*, *118*(7), 3260–3277. https://doi.org/10.1002/jgrc.20244

Tessin, A., März, C., Blais, M.-A., Brumsack, H.-J., Matthiessen, J., O'Regan, M., & Schnetger, B. (2020). Arctic continental margin sediments as possible Fe and Mn sources to seawater as sea ice retreats: Insights from the Eurasian margin. *Global Biogeochemical Cycles*, *34*(8), e2020GB006581. https://doi.org/10.1029/2020GB006581

Tovar-Sánchez, A., Duarte, C. M., Alonso, J. C., Lacorte, S., Tauler, R., & Galbán-Malagón, C. (2010). Impacts of metals and nutrients released from melting multiyear Arctic sea ice. *Journal of Geophysical Research*, *115*(C7). https://doi.org/10.1029/2009JC005685

Tuerena, R. E., Hopkins, J., Buchanan, P. J., Ganeshram, R. S., Norman, L., von Appen, W.-J., et al. (2021). An Arctic Strait of two halves: The changing dynamics of nutrient uptake and limitation across the fram Strait. *Global Biogeochemical Cycles*, *35*(9), e2021GB006961. https://doi.org/10.1029/2021GB006961

Twining, B. S., & Baines, S. B. (2013). The trace metal composition of Marine Phytoplankton. *Annual Review of Marine Science*, *5*(1), 191–215. https://doi.org/10.1146/annurev-marine-121211-172322

Våge, S., Basedow, S. L., Tande, K. S., & Zhou, M. (2014). Physical structure of the Barents Sea Polar Front near Storbanken in August 2007. *Journal of Marine Systems*, *130*, 256–262. https://doi.org/10.1016/j.jmarsys.2011.11.019

Vancoppenolle, M., Bopp, L., Madec, G., Dunne, J., Ilyina, T., Halloran, P. R., & Steiner, N. (2013). Future Arctic Ocean primary productivity from CMIP5 simulations: Uncertain outcome, but consistent mechanisms. *Global Biogeochemical Cycles*, *27*(3), 605–619. https://doi.org/10.1002/gbc.20055

van Genuchten, C. M., Hopwood, M. J., Liu, T., Krause, J., Achterberg, E. P., Rosing, M. T., & Meire, L. (2022). Solid-phase Mn speciation in suspended particles along meltwater-influenced fjords of West Greenland. *Geochimica et Cosmochimica Acta*, *326*, 180–198. https://doi.org/10.1016/j.gca.2022.04.003

van Genuchten, C. M., Rosing, M. T., Hopwood, M. J., Liu, T., Krause, J., & Meire, L. (2021). Decoupling of particles and dissolved iron downstream of Greenlandic glacier outflows. *Earth and Planetary Science Letters*, *576*, 117234. https://doi.org/10.1016/j.epsl.2021.117234

van Pelt, W., & Frank, T. (2025). New glacier thickness and bed topography maps for Svalbard. *The Cryosphere*, *19*(1), 1–17. https://doi.org/10.5194/tc-19-1-2025

Vivier, F., Lourenço, A., Michel, E., Skogseth, R., Rousset, C., Lansard, B., et al. (2023). Summer hydrography and circulation in Storfjorden, Svalbard, following a record low Winter sea-ice extent in the Barents Sea. *Journal of Geophysical Research: Oceans*, *128*(2), e2022JC018648. https://doi.org/10.1029/2022JC018648

von Langen, P. J., Johnson, K. S., Coale, K. H., & Elrod, V. A. (1997). Oxidation kinetics of manganese (II) in seawater at nanomolar concentrations. *Geochimica et Cosmochimica Acta*, *61*(23), 4945–4954. https://doi.org/10.1016/S0016-7037(97)00355-4

Wehrmann, L. M., Formolo, M. J., Owens, J. D., Raiswell, R., Ferdelman, T. G., Riedinger, N., & Lyons, T. W. (2014). Iron and manganese speciation and cycling in glacially influenced high-latitude fjord sediments (West Spitsbergen, Svalbard): Evidence for a benthic recycling-transport mechanism. *Geochimica et Cosmochimica Acta*, *141*, 628–655. https://doi.org/10.1016/j.gca.2014.06.007

Wu, J., Boyle, E., Sunda, W., & Wen, L.-S. (2001). Soluble and colloidal iron in the oligotrophic north Atlantic and north Pacific. *Science*, *293*(5531), 847–849. https://doi.org/10.1126/science.1059251

Wu, M., McCain, J. S. P., Rowland, E., Middag, R., Sandgren, M., Allen, A. E., & Bertrand, E. M. (2019). Manganese and iron deficiency in Southern Ocean Phaeocystis Antarctica populations revealed through taxon-specific protein indicators. *Nature Communications*, *10*(1), 3582. https://doi.org/10.1038/s41467-019-11426-z

Yeats, P. A., & Strain, P. M. (1990). The oxidation of manganese in seawater: Rate constants based on field data. *Estuarine, Coastal and Shelf Science*, *31*(1), 11–24. https://doi.org/10.1016/0272-7714(90)90025-M

Zhang, R., John, S. G., Zhang, J., Ren, J., Wu, Y., Zhu, Z., et al. (2015). Transport and reaction of iron and iron stable isotopes in glacial meltwaters on Svalbard near Kongsfjorden: From rivers to estuary to ocean. *Earth and Planetary Science Letters*, *424*, 201–211. https://doi.org/10.1016/j.epsl.2015.05.031

Zhu, X., Hopwood, M. J., Laufer-Meiser, K., & Achterberg, E. P. (2024). Incubation experiments characterize turbid Glacier plumes as a major source of Mn and Co, and a minor source of Fe and Si, to seawater. *Global Biogeochemical Cycles*, *38*(10), e2024GB008144. https://doi.org/10.1029/2024GB008144

References From the Supporting Information

Abrahamsen, E. P., Meredith, M. P., Falkner, K. K., Torres-Valdes, S., Leng, M. J., Alkire, M. B., et al. (2009). Tracer-derived freshwater composition of the Siberian continental shelf and slope following the extreme Arctic summer of 2007. *Geophysical Research Letters*, *36*(7). https://doi.org/10.1029/2009GL037341

Berger, C. J. M., Lippiatt, S. M., Lawrence, M. G., & Bruland, K. W. (2008). Application of a chemical leach technique for estimating labile particulate aluminum, iron, and manganese in the Columbia River plume and coastal waters off Oregon and Washington. *Journal of Geophysical Research*, *113*(C2). https://doi.org/10.1029/2007JC004703

Ekwurzel, B., Schlosser, P., Mortlock, R. A., Fairbanks, R. G., & Swift, J. H. (2001). River runoff, sea ice meltwater, and Pacific water distribution and mean residence times in the Arctic Ocean. *Journal of Geophysical Research*, *106*(C5), 9075–9092. https://doi.org/10.1029/1999JC000024

Epstein, S., & Mayeda, T. (1953). Variation of O18 content of waters from natural sources. *Geochimica et Cosmochimica Acta*, *4*(5), 213–224. https://doi.org/10.1016/0016-7037(53)90051-9

López-Sandoval, D. C., Delgado-Huertas, A., & Agustí, S. (2018). The 13C method as a robust alternative to 14C-based measurements of primary productivity in the Mediterranean Sea. *Journal of Plankton Research*, *40*(5), 544–554. https://doi.org/10.1093/plankt/fby031

Meredith, M., Heywood, K., Dennis, P., Goldson, L., White, R., Fahrbach, E., et al. (2001). Freshwater fluxes through the Western Fram Strait. *Geophysical Research Letters*, *28*(8), 1615–1618. https://doi.org/10.1029/2000GL011992

Winsborrow, M. C. M., Patton, H., & Esteves, M. (2022). Chapter 8—The eurasian Arctic. In D. Palacios, P. D. Hughes, J. M. García-Ruiz, & N. Andrés (Eds.), *European glacial landscapes* (pp. 59–64). Elsevier. https://doi.org/10.1016/B978-0-12-823498-3.00036-4